Chemical Engineering Journal Advances 26 (2026) 101081

Contents lists available at ScienceDirect

Chemical Engineering Journal Advances

journal homepage: www.sciencedirect.com/journal/chemical-engineering-journal-advances

Light transfer investigation in solar tubular photobioreactors using Monte Carlo ray tracing

J. Hoeniges [a,b], L. Pilon [b], J. Dauchet [c], J. Pruvost [*,a]

[a] Nantes Université, Oniris, CNRS, GEPEA, UMR 6144, Saint-Nazaire, France
[b] University of California Los Angeles, Henry Samueli School of Engineering and Applied Science, Mechanical and Aerospace Engineering Department, 420 Westwood Plaza, Los Angeles, CA 90095, USA
[c] Université Clermont Auvergne, Clermont Auvergne INP, CNRS Institut Pascal, F-63000 Clermont-Ferrand, France

ARTICLE INFO

Keywords:
Modeling
Photobioreactors
Tubular
Microalgae
Light transfer
Ray-tracing

ABSTRACT

Tubular photobioreactors (PBRs) are widely used for microalgae solar culture. In such geometry, light transfer is rendered complex by the effects of refractive index mismatches across curved air/glass/culture interfaces. This study aims to develop an open source code implementing the Monte Carlo ray-tracing (MCRT) method and to identify the design rules to optimize light transfer in tubular PBRs. The light transfer model accounted for the tube wall thickness, the angle of the collimated and diffuse incident solar radiation, the multiple reflections and refractions at interfaces, and anisotropic scattering and absorption by the microalgae cells. The importance of the dimensionless optical thickness of the suspension and of the tube thickness normalized by the outer tube radius in determining the radiation field was demonstrated. The concave tube wall was responsible for light concentration and a normalized tube thickness in the range 0.2–0.4 was found to be optimum to increase photon flux in the culture by up to 42 % and the biomass productivity by 60 % compared to very thin tube thickness. Furthermore, due to the effect of curved optical surfaces, the conditions for maximum growth rate were different from those for full light absorption without dark volume, by contrast with flat panel PBRs. Predictions for several PBR configurations confirmed the usefulness of our MCRT method as a generic tool to predict performances of solar tubular PBRs. For example, an increase of 60 % in maximum biomass concentration was obtained with vertical inclination of PBR tubes compared to horizontal inclination, but with an increase in light stressing conditions.

1. Introduction

Innovations at the nexus of food, energy, and water systems will be crucial to confront the difficulties posed by the climate crisis [1]. In particular, photosynthetic microalgae have garnered interest as a fast-growing crop for human and animal feed [2], as a source of biomass for carbon-neutral biofuels [3], and as a valuable ingredient in food supplements, nutraceuticals, and cosmetics [4]. Although microalgae grow naturally in a variety of environments such as lakes, ponds, and oceans, harnessing their potential as a sustainable resource requires industrial-scale cultivation which poses a number of technical challenges [5]. Cultivation systems must efficiently deliver light and nutrients to the microalgae, while maintaining other parameters such as temperature, pH, and dissolved O_2 at or near their optimum operating points.

Microalgae cultivation systems are frequently classified as either open or closed. Raceway ponds are the most commonly used form of open system. This approach features relatively low construction and operating costs and is thus the most widespread method for large-scale microalgae cultivation [6]. In contrast to open systems, closed microalgae cultivation systems or photobioreactors (PBRs) feature lower risk of contamination and higher biomass productivity. Although closed systems are more expensive, they offer the possibility of total control over the physiological conditions [7]. This enables closed PBRs to attain higher values of biomass productivity or to be used to apply a certain set of growth conditions to favor the production a specific molecule [8].

Closed systems come in a wide range of geometries including tubular, and flat-panel PBRs. Tubular PBR has become prevalent in recent years in many industrial installations. This is mainly due to its ease of scaling and availability of long transparent tubes, enabling the construction of large-scale solar installations [9].

* Corresponding author.
E-mail address: jeremy.pruvost@univ-nantes.fr (J. Pruvost).

https://doi.org/10.1016/j.ceja.2026.101081

Available online 6 February 2026

NOMENCLATURE

A	Specific rate of photon absorbed [μmol.s^{-1}. kg ^{3}]
A_c	Specific rate of photon absorbed at compensation point [μmol.s^{-1}.kg^{-1}]
a_{light}	Specific illuminated area for the photobioreactor [m^{-1}]
b	Back-scattered fraction for radiation [dimensionless]
C_X	Biomass concentration [kg.m^{-3}]
C_X / a_{light}	Optical thickness [kg.m^{-2}]
$\overline{A}_{abs}$	Mass absorption coefficient [m^2.kg^{-1}]
$\overline{S}_{sca}$	Mass scattering coefficient [m^2.kg^{-1}]
Eray	Amount of energy per ray [μmol.s^{-1}.m^{-2}]
g	microalgae cell asymmetry factor [dimensionless]
G	Local spherical irradiance [μmol.s^{-1}.m^{-2}]
I	Intensity [μmol.s^{-1}.m^{-2}.sr^{-1}]
J_{O2}	specific rate of oxygen production or consumption [$mol_{O_2} kg_X^{-1} s^{-1}$]
K	Half saturation constant for photosynthesis [μmol.s^{-1}. m^{-2}]
L	Depth of flat panel photobioreactor [m]
n	refractive index [dimensionless]
Nrays	Number of rays [dimensionless]
p	Photon location in the MCRT approach
q	Hemispherical photon flux density on a given surface (PFD) [μmol.s^{-1}.m^{-2}]
r_i	Inner radius of the tube [m]
r_o	Outer radius of the tube [m]
r_s	Biomass areal growth rate (productivity) [kg.m^{-2}.s^{-1} or g. m^{-2}.day^{-1}]
r_X	Biomass volumetric growth rate (productivity) [kg.m^{-3}. s^{-1} or kg.m^{-3}.day^{-1}]
S_{light}	Illuminated surface of the photobioreactor [m^2]
t	Tube wall thickness [m]
t/r_o	Normalized wall thickness [dimensionless]
z	Depth of culture or length [m]

Greek letters

α	Linear scattering modulus [dimensionless]
β	Inclination of the photobioreactor surface[°]
γ	Illuminated light fraction [dimensionless]
δ	Extinction coefficient for the two-flux method [m^{-1}]
θ	Incident angle (defined from the outward normal of the illuminated surface of the culture system)
ρ_M	Maximum energy yield for photon conversion [dimensionless]
$\overline{\varphi}$	Mean mass quantum yield for the Z-scheme of photosynthesis [$kg_X.\mu mol_{h\nu}^{-1}$]

Subscripts

//	Related to direct radiation
⊥	Related to normal direct radiation
∩	Related to total diffuse radiation
cult	Related to the culture volume
col	Related to collimated light
dif	Related to diffuse light
in	Related to the the PBR surface

A. bbreviations

LRPA	Local Rate of Photons Absorption
MCRT	Monte Carole Ray Tracing
MRPA	Mean Rate of Photons Absorption
PBR	Photobioreactor
PFD	Photon flux density

The ability of PBR technology to control growing conditions means that light contribution to the cultivation system becomes a determining factor in PBR performance. Thus, when all growing conditions are controlled, the so-called "light-limited culture" is achieved, meaning that culture performance for a given strain depends solely on the amount of light captured and its photosynthetic utilization within the culture volume [10]. Radiative models that calculate light transfer within the substrate then become essential for the scaling and optimization of PBR technologies. This is particularly true when using sunlight. The light source then becomes variable, both in intensity and in its position relative to the culture system, resulting in variations in the angle of incidence that directly affect light penetration into the culture volume and the resulting growth [11,12].

For tubular PBRs, light transfer is more complex due to the effect of curved air/glass/culture interfaces, which induce refraction and reflection of incident light on each optical surface of the tubular geometry. Consequently, the curvature and wall thickness of the tube influence the light transferred to the culture. Furthermore, regardless of the culture system, it is well established that, due to light attenuation by the microalgae culture medium, a small culture depth is preferable (generally a few centimeters or less, [10,13]). As a result, the tube wall thickness could be of the same order of magnitude as the culture depth, which could increase its influence on light transferred to the culture volume.

Light transfer through a well-mixed suspension of microalgae is governed by the radiative transfer equation (RTE) for a homogeneous absorbing, scattering, and non-emitting medium. Frequently, for flat-panel photobioreactors (PBRs) or raceway ponds, the two-flux approximation is used to obtain an analytical solution to the one-dimensional RTE [14–16]. This approximation has been used extensively [14–18] and has been successfully validated against results from a 3D RTE solvers for ponds and flat-panel PBRs [15].

For tubular PBRs, Cornet et al. [18] applied the two-flux approximation to obtain a one-dimensional solution of the radiative transfer equation for a non-emitting medium and absorbing and scattering cells. The incident radiation was assumed to be radially homogeneous and scattering by the cells was assumed to be isotropic. A reformulation of this approach was presented by Takache et al. [19] for the case of anisotropic scattering and low biomass concentration. However, these solutions were developed to model artificially illuminated PBRs. Under solar conditions, tubular PBRs are illuminated on a single side and the case of homogeneous radial illumination is not realistic. Thus, methods for solving the two- or three-dimensional RTE are necessary for accurate predictions of the radiative field within the culture.

Slegers et al. [20] predicted the yearly biomass productivity of vertical and horizontally oriented tubular PBRs using solar conditions for locations in The Netherlands, France, and Algeria. Their model accounted for diffuse and collimated incidence, tube reflectance, and tube mutual shading. The impact of ground reflectance, tube material and tube spacing were also considered. Here, the local fluence rate within the culture was predicted assuming that the light path was normal to the reactor walls. However, previous studies have demonstrated that the angle of incidence of light on a microalgae culture has a significant impact on the local rate fluence rate and the resulting predicted growth rate [11].

Lee et al. [15] solved the three-dimensional RTE using a discrete Galerkin method [21] for a horizontal tubular PBR aligned with the North/South axis. The local fluence rate and corresponding microalgae growth rate were predicted for solar intensities in Los Angeles, CA on June 21st. The incident solar flux was composed of collimated and

diffuse light. The results demonstrated the same scaling relationship as observed theoretically in Hoeniges et al. [22]. Predicted areal productivity was found to be directly related to the product of the culture biomass concentration C and the PBR radius r_i, introducing the relevance of areal concentration or optical thickness (both being similar and expressed in kg m^{-2}) as a scaling parameter. Here, a single PBR orientation was considered and any reflection and/or refraction effects at the air/tube or tube/culture interfaces were neglected.

Marotta et al. [23] developed a Monte Carlo ray-tracing (MCRT) method to investigate the effect of refraction at the air/culture interface on the radiative field within a horizontal tubular PBR. The incident light was collimated and normally incident with respect to the longitudinal axis of the tube. The presence of the tube walls was neglected, and the reactor was modeled as a cylinder of water in air with refractive indices of 1.33 and 1.0, respectively. Reflection events at the water/air interface and scattering by the microalgae cells were neglected. Radiative transfer in the microalgae culture was modeled according to Beer-Lambert's law. The simulated results of the radiative field predicted the presence of dark volumes in the tube due to refraction at the air/liquid interface. This phenomenon was more pronounced for lower biomass concentrations where the light was not fully attenuated. Indeed, at very low biomass concentration ($C_X = 0.02$ kg m^{-3}) refraction at the air/liquid interface led to a light concentrating effect where the predicted local rate of photon absorption at the back of the tube was larger than that near the illuminated surface of the tube. Nonetheless, the total fraction of photons absorbed was only slightly changed when reflection and refraction at the air/liquid interface were accounted for. Finally, the photon distribution was observed to scale with the factor Cr_i.

Ryma et al. [24] presented a rigorous MCRT approach to simulate the radiation field in a solar tubular PBR. This approach took into account the position and angle of incidence of the sun, direct and diffuse light, as well as possible reflections and refractions on the wall. It also enabled the prediction of variations in light received by microalgae as a function of mixing conditions. To do so, the determination of the radiation field was coupled with a discrete Lagrangian random walk to track the cells. However, given the large diameter of the tube, the wall thickness was not taken into account.

Thus, while light transfer in tubular PBRs has been previously investigated, to the best of our knowledge, no study has considered the impact of tube wall thickness on the light distribution and predicted microalgae growth. Indeed, the thickness of the tube wall is in most cases relatively small for typical tubular PBRs with a radius on the order of few centimeters or decimeter. However, in the case of thin-tube PBRs (i.e. for tube diameter below few centimeters, where tube wall thickness could be in the same order of magnitude, or even greater, compared to the outer tube radius).

Therefore, the goal of the current numerical study was to propose a generic model to predict light transfer and microalgae growth rate within solar tubular PBRs, taking into account the influence of the tube wall thickness. This MCRT model (which was made available as an open source code via a public share on GitHUB [25]) was developed to consider all relevant optical phenomena involved in tubular PBRs. It accounted then for diffuse and collimated radiations, non-normal incidence, multiple reflection and refraction events at all optical interfaces, and absorption and anisotropic scattering by the microalgae cells in suspension. The MCRT model was then used to numerically investigate the impact of tube diameter as well as wall thickness, light incidence angle and scattering by the microalgae on the PBR illuminated fraction and resulting microalgae growth. Finally, the daily biomass productivity was predicted for several different PBR inclination angles and orientations for solar conditions corresponding to typical winter and summer days in Saint-Nazaire, France. All simulations enabled to identify practical guidelines for scaling-up and optimizing the design and operation of tubular outdoor PBRs.

2. Methods

2.1. Problem statement

Let us consider a tubular PBR of outer radius r_o and inner radius r_i containing a microalgae culture of biomass concentration C_x and exposed on a single side to a diffuse I_{dif} and collimated intensity I_{col} with an incidence angle represented by θ_{in} taken with respect to the orthogonal vector of the tube's longitudinal axis (Fig. 1). Hence, the incident hemispherical photon flux density (PFD), representing the averaged photon flux density received onto the PBR outer surface facing the sun, was taken as $q''_{in} = (2/\pi)I_{col}cos(\theta_{in}) + \pi I_{dif}$ (see Appendice). The tube wall thickness t was given by $t = r_o - r_i$. The PBR inclination angle β was measured with respect to the horizontal axis (i.e. ground).

The tube was considered to be non- absorbing with a refractive index representative of that of glass i.e., n_t =1.5. The culture medium was also assumed to be non-absorbing, with a refractive index representative of that of water, i.e., $n_c = 1.33$.

Chlorella vulgaris, whose radiative properties and growth modeling have already been characterized and validated under similar conditions, was chosen as the model species [11]. The culture was comprised of a suspension of *C. vulgaris* cells with PAR-averaged mass absorption $\overline{A}_{abs}$ and scattering $\overline{S}_{sca}$ cross-sections taken from Soulies et al. [11] as in Hoeniges et al. [22]. Here, the asymmetry factor g was taken as 0.974 according to the measured value reported for *C. vulgaris* in [11,26]. Note that the MCRT method described below could be applied to any other species of microalgae, provided that the radiative properties (mass absorption $\overline{A}_{abs}$ and scattering $\overline{S}_{sca}$ cross-sections, asymmetry factor g) are known.

3. Methods

3.1. Assumptions

Light transfer within the tubular PBR was modeled using the Monte-Carlo ray-tracing method [27–32]. To do so, the following assumptions were made [30]:

(i) The tube wall thickness was much larger than the wavelength of radiation in the PAR region such that geometric optics prevailed.
(ii) Both the tube wall and the microalgae culture medium were considered to be non-absorbing over the PAR region.
(iii) Refractive indices of the air, tube wall, and culture medium were taken as constant over the PAR region. Furthermore, each of these components was considered to be non-emitting and non-scattering.
(iv) All interfaces were considered in the absence of deposits or biofilms. This assumption is important because biofilm formation is a known problem in PBR culture, particularly in tubular PBRs [33]. This could be addressed by introducing, for example, an additional interface exhibiting both deposit and biofilm properties. Given the diversity of possible scenarios, this option was not retained.
(v) All interfaces were taken as optically smooth. In other words, the surface roughness was much less than the wavelength of the light in the photosynthetically active radiation (PAR) region (λ = 400 - 700 nm) such that reflection and transmission were specular. Then a photon incident at an angle θ_1, measured with respect to the interface normal vector, upon an interface between two non-absorbing media of refractive indices n_1 and n_2, respectively, underwent refraction and was transmitted at angle θ_2 given by Snell's law, i.e. [34]:

$$\theta_2 = \mathrm{asin}\left(\sin(\theta_1)\frac{n_1}{n_2}\right) \quad (1)$$

Then, the reflectivity, which represents the probability that said

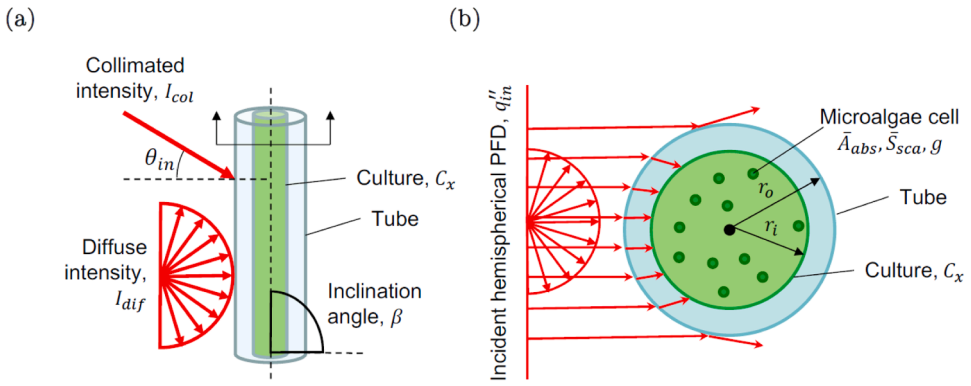

Fig. 1. (a) Side view and (b) section view of a simplified representation of the tubular photobioreactor considered in the current study.

photon is reflected instead of transmitted, can be given by Fresnel's equation, i.e., [35]:

$$\rho = \frac{1}{2}\left[\frac{\tan^2(\theta_1-\theta_2)}{\tan^2(\theta_1+\theta_2)}+\frac{\sin^2(\theta_1-\theta_2)}{\sin^2(\theta_1+\theta_2)}\right] \quad (2)$$

Predictions of the light transfer and microalgae growth within the PBR were based on the assumptions that:

(vi) the PBR was operated in the light-limited regime wherein growth was only a function of the amount of light available to the microalgae cells [11,15,36]. Thus the PBR was not limited by any other

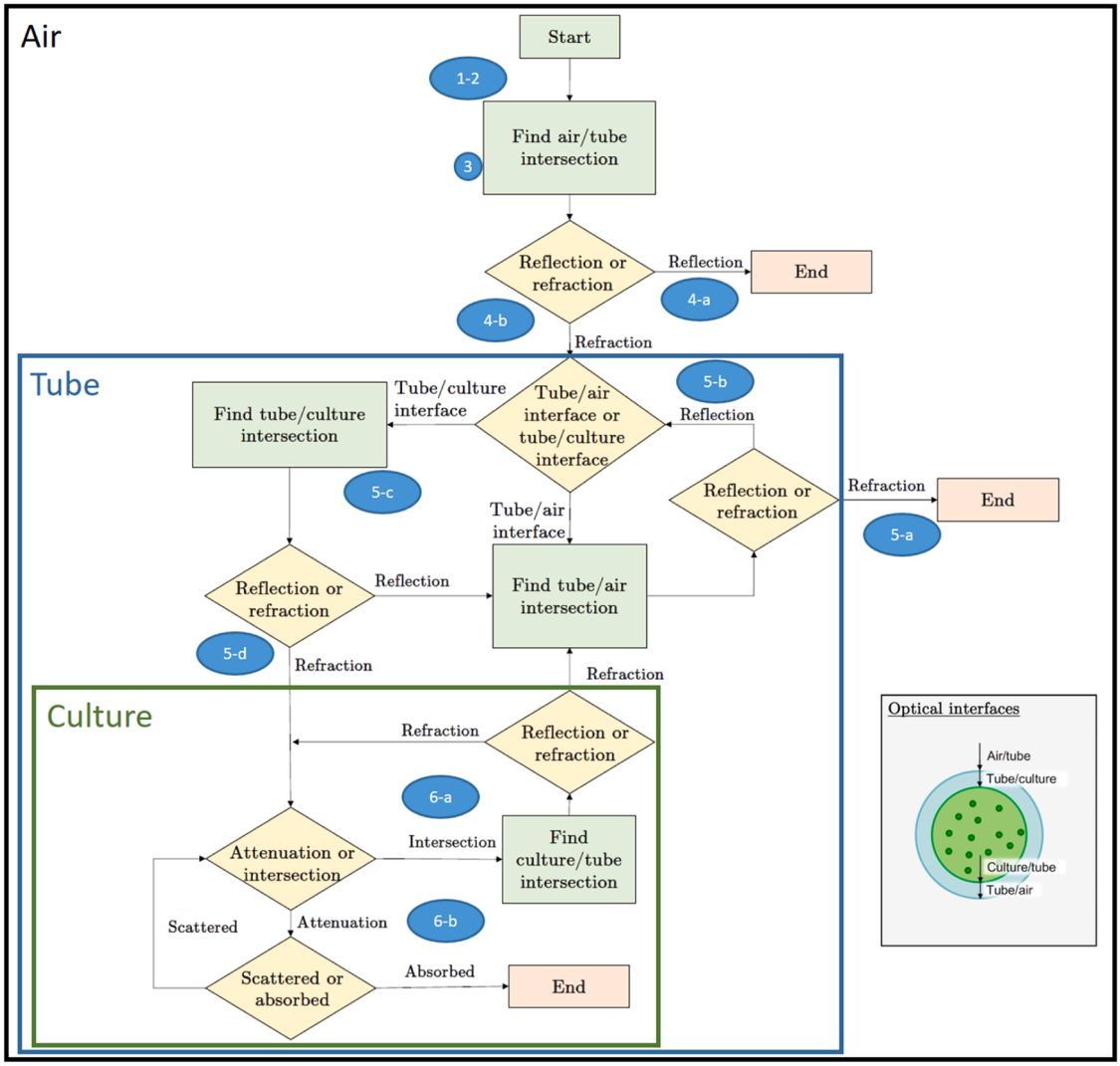

Fig. 2. A simplified flow chart of the algorithm structure used to track a ray as it propagates through the tubular photobioreactor where it may experience multiple reflection, refraction, and scattering events before being transmitted or absorbed in the microalgae culture (the numbering refers to the description of the flowchart in the text).

operating parameters such as temperature, pH, nutrient availability, or dissolved oxygen concentration.
(vii) The microalgae culture was well-mixed with uniform biomass concentration C_X throughout the PBR.
(viii) The tube was considered to be infinitely long such that edge effects at the top and bottom of the PBR were neglected and the light transfer within the tube was two-dimensional. In other words for a given case the local fluence rate was only a function of the x and y coordinates.

3.2. Monte Carlo ray-tracing method

In order to predict the local rate of photon absorption (LRPA) for a microalgae culture within a tubular PBR, a Monte Carlo ray-tracing (MCRT) method was used [28,30,31,37]. A large number N_{rays} of discrete photon bundles or "rays" were incident upon the tubular PBR. The incident photon bundles could undergo multiple refraction and reflection events at the air/tube, tube/culture, culture/tube, and tube/air interfaces, as well as scattering and absorption events in the microalgae culture. The rays were tracked until they were either (i) reflected away from the PBR, (ii) transmitted through the PBR, or (iii) absorbed in the microalgae culture. The step-by-step process is outlined in the flow diagram in Fig. 2 and was as follows:

1. Randomly generate an emission location $p_0 = (x_0; y_0; z_0)$ on the plane in front of the tube.
2. Determine ray direction vector s_i based on the incidence angle θ_{in}
3. Calculate the intersection location p_0 between the ray and the outer air/tube interface and the reflectance ρ of the air/tube interface based on the incidence angle θ_{in} between the ray and the outward pointing normal vector of the tube surface using the generalized Fresnel's equations (see Eq. (2)).
4. Generate a random number R between 0 and 1 from the uniform distribution.
(a) If $R < \rho$ ray is reflected, terminate ray
(b) Else if $R > \rho$ ray is refracted, calculate the new ray direction s_t according to Snell's law (see Eq. (1)) and continue.
5. Calculate new intersection location p' on either (i) the tube/air interface or (ii) the tube/culture interface. Calculate the corresponding reflectance ρ and generate random number R.
(a) If intersection is on the tube/air interface and ray is refracted, terminate ray.
(b) If intersection is on the tube/air interface and ray is reflected, calculate the new ray direction s_t according to specular reflection and return to Step 5.
(c) If intersection is on the tube/culture interface and ray is reflected, calculate new intersection location on tube/air interface p', new direction s_r according to specular reflection and new reflectance ρ, return to Step 5.a or 5.b according to random number outcome.
(d) If intersection is on the tube/culture interface and ray is refracted, ray enters microalgae culture. Calculate new intersection location p_0 and direction s_t according to Snell's law and continue.
6. For rays that enter the microalgae culture, calculate the distance l_{geo} between current p' and next p'' intersection location at the culture/tube interface. Calculate the probable path length l_β traveled before attenuation in the culture using the culture extinction coefficient, $\beta_{ext} = C_X(\overline{A}_{abs} + \overline{S}_{sca})$ according to

$$l_\beta = -In(R)/\beta_{ext} \tag{3}$$

(a) If $l_\beta > l_{geo}$, ray intersects culture/tube interface before attenuation occurs. Set intersection location $p' = p''$.
i. If refraction occurs, calculate new direction s_t according to Snell's laws, new intersection location on tube/air interface p', and new reflectance ρ. Return to Step 5.a or 5.b according to reflectance ρ and random number outcome.
ii. If reflection occurs, calculate new direction s_r according to specular reflection and update the distance until attenuation according to $l_\beta = l_\beta - l_{geo}$. Return to Step 6 without re-calculating the attenuation distance l_β.
(b) Else if $l_\beta < l_{geo}$, attenuation occurs at a location a distance of l_β along the current propagation direction from its last attenuation, reflection, or refraction event at p'. Use the culture single-scattering albedo $\omega = \overline{S}_{sca}/(\overline{A}_{abs} + \overline{S}_{sca})$ and a random number R between 0 and 1 to determine if ray is scattered or absorbed.
i. If $R < \omega$, ray is scattered. A new scattered direction s_{sca} is defined by a randomly generated azimuthal ψ_{sca} angle and a polar θ_{sca} angle generated by using a new random number R and the integrated accumulated distribution of the Henyey-Greenstein function, i.e., [32]

$$cos(\theta_{sca}) = \frac{1}{2g}\left\{1 + g^2 - \left(\frac{1+g^2}{1+gs}\right)^2\right\} \tag{4}$$

where s = 2R - 1. Return to Step 6.

ii. If $R > \omega$, ray is absorbed and the absorption location $p_{abs} = (x_{abs}, y_{abs})$ is recorded.

The above process was completed for a large number of rays, until each ray was either reflected or transmitted away from the PBR or absorbed at given location $p_{abs} = (x_{abs}, y_{abs})$. Recall that the radiative field within the tube was assumed to be independent of the z-direction. The cross-section of the tube was discretized into a $N_{el} \times N_{el}$ rectangular mesh featuring square elements of width $\Delta y = \Delta x = 2r_i/N_{el}$. A matrix $[N_{abs}]$ was defined wherein each element $(i; j)$ contained the number of rays absorbed $N_{abs,i,j}$ at a location $p_{abs} = (x_{abs}, y_{abs})$ such that $x_{i-1} < x_{abs} < x_i$ and $y_{i-1} < y_{abs} < y_i$ where x_i and y_i represent the right-hand and upper element boundaries, respectively, of element (i, j).

Each ray can be said to carry an amount of energy E_{ray} equal to

$$E_{ray} = \frac{S_{light} q''_{in}}{N_{rays}} \tag{5}$$

where S_{light} is the illuminated surface area, given by $S_{light} = \pi r_o H$ for illumination on a single side and H is the tube height considered. Then, the specific local rate of photon absorption A (x, y) in $\mu mol_{h\nu} kg^{-1} s^{-1}$ (LRPA) can be calculated from the ray absorption matrix $[N_{abs}]$ according to

$$A(x_i, y_i) = \frac{N_{abs,i,j} E_{ray}}{V_{ej} C_x} \tag{6}$$

where V_{el} is the element volume given by $\Delta x^2 H$. Note that the tube height H is contained in both the E_{ray} and V_{el} terms and will thus cancel yielding results that are independent of the tube height considered.

Once determined, the spatial distribution of the LRPA A (x, y) can be used to calculate the illuminated fraction γ, where γ is the ratio of the illuminated volume to the total volume of the culture [19,38]:

$$\gamma = \frac{S(A > A_c)}{\pi r_i^2} \tag{7}$$

where $S(A > A_c)$ is the cross-sectional area of the tube where the local rate of photon absorption was greater than the compensation rate of photon absorption A_c, and so representing the part of cross-sectional area of the tube where LRPA value is sufficient to have positive growth (i.e. local values of J_{O_2} in Eq. 10 are positive).

The PAR- averaged local fluence rate $G(x, y)$ in $\mu mol_{h\nu} m^{-2} s^{-1}$ can

then be determined by simply dividing the LRPA by the PAR-averaged mass absorption cross-section $\overline{A}_{abs}$(in $m^2 kg_X^{-1}$):

$$G(x,y) = \frac{A(x,y)}{\overline{A}_{abs}} \tag{8}$$

In the case of solar simulations, the incident hemispherical PFD q''_{in} was composed of both collimated (i.e. direct) radiation and diffuse radiation. In this case, the MCRT algorithm was executed twice, once for collimated PFD and once for diffuse PFD yielding two separate matrices containing the local rate of photon absorption, denoted by [A $_{col}$] and [A $_{dif}$]. The two matrices were superimposed to calculate the total LRPA and the corresponding spatially averaged value MRPA (for Mean Rate of Photons Absorption) according to [15]:

$$[A] = [A\ col] + [A\ dif] \text{with} MRPA = \frac{1}{S}\cdot\int A(x,y)dS \tag{9}$$

Here S is the cross-sectional area of the culture volume in the tubular PBR given by πr_i^2.

It is worth noting that our MCRT method could be readily extended to more complex cases. For example, Zheng et al. [39] used a MCRT method to determine the view factors between the external surface of cylindrical PBRs and sky/ground surfaces arranged in different array configurations. This method allowed to account for the effects of spacing between the PBRs and different layouts configurations. This work could lead to the extension of our MCRT model by allowing to determine the light received by the surface of PBRs for more complex tubular configurations (then used as an input in our model). As another example, Pozzobon [40] used a MCRT method to determine the contribution of bubbles to the radiation field in an airlift PBR. Although the geometry is not tubular, this approach could prove complementary to our work, particularly for introducing the influence of bubbles in vertical tubular PBRs.

3.3. Microalgae growth kinetics

The microalgae growth kinetics model for *Chlorella vulgaris* already published elsewhere [11] was used to predict the growth rate as a function of the LRPA. First, the volume-averaged specific rate of oxygen production or consumption $\langle J_{O_2}(t)\rangle$ (in $mol_{O_2} kg_X^{-1} s^{-1}$) as a function of the LRPA A(x, y) was calculated according to:

$$\langle J_{O_2}(t)\rangle = \int_S \left[\rho_M \frac{K_A}{K_A + A(x,y)} \overline{\phi}'_{O_2} A(x,y) - \frac{J_{NADH_2}}{\nu_{NADH_2-O_2}} \frac{K_r}{K_r + A(x,y)}\right] dS \tag{10}$$

Here, ρ_M is the maximum energy yield for photon conversion, $\overline{\phi}'_{O_2}$ is the molar quantum yield of O_2 for the Z-scheme of photosynthesis, K_A is the half-saturation constant for photosynthesis, J_{NADH_2} is the specific rate of cofactor regeneration on the respiratory chain related to the oxygen consumption by the stoichiometric coefficient of cofactor regeneration on the respiratory chain $\nu_{NADH_2-O_2}$ and K_r is a saturation constant describing the inhibition of respiration in light.

Then, the stoichiometric relationship between the production of oxygen and the production of biomass was used to predict the volume-averaged growth rate $\langle r_X(t)\rangle$ (in $kg_X.m^{-3}s^{-1}$) as a function of $\langle J_{O_2}(t)\rangle$:

$$\langle r_X(t)\rangle = \langle J_{O_2}(t)\rangle \frac{M_X C_X(t)}{\nu_{O_2-X}} \tag{11}$$

The relevant parameters for the growth kinetics model can be found in Table 1. Please note that applying this method to another microalgae species would require recalibrating the parameters (more information can be found in [17]).

Table 1
Growth kinetics parameters for *Chlorella vulgaris (Soulies et al., 2016)*.

Parameter	*Value*	*Unit*
υ_{O_2-X}	0.8	
J_{NADH_2}	2.8×10^{-3}	$mol_{NADH_2} kg_X^{-1} s^{-1}$
υ_{O_2-X}	1.13	
		$1231^1 mol_{O2} \mu mol_{h\nu}$
$\overline{\phi}'_{O_2}$	1.1×10^{-7}	$mol_{O_2} \mu mol_{h\nu}^{-1}$
M_X	0.024	$kg_X mol_C^{-1}$
$\upsilon_{NADH_2-O_2}$	2	
K_A	40,000	$\mu mol_{h\nu} kg^{-1} s^{-1}$
K_r	556.5	$\mu mol_{h\nu} kg^{-1} s^{-1}$
A_C	2800	$\mu mol_{h\nu} kg^{-1} s^{-1}$

3.4. Comparison with a canonical approximate solution for radiative transfer in cylindrical PBRs

In the case of quasi-collimated, radially incident light, the radiative field within a tubular PBR can be approximated by applying the two-flux method to the one-dimensional radiative transfer equation in cylindrical coordinates. This approximation is more accurate for high biomass concentrations, even though it has been extended to lower optical thicknesses by Takache et al [19] who obtained the expression:

$$\frac{G(r)}{q''_{in}} = 2\frac{I_0(\delta r)}{I_0(\delta r_i) + \alpha I_1(\delta r_i)} \tag{12}$$

where $I_0(r)$ and $I_1(r)$ represent the zero- and first-order modified Bessel functions of the first kind where the radial coordinate r is defined with respect to the tube center, and the extinction coefficient for the two-flux method δ is given by:

$$\delta = \alpha C_X(\overline{A}_{abs} + 2b\overline{S}_{sca}) \text{ with } \alpha = \sqrt{\frac{\overline{A}_{abs}}{\overline{A}_{abs} + 2b\overline{S}_{sca}}} \tag{13}$$

where b is the PAR-averaged back scattering ratio.

To compare the current MCRT method with this analytical approximate solution that is widely used in the study of cylindrical PBRs, the local fluence rate $G(r)$ was predicted for an example case using PBR geometry and microalgae radiative properties from Takache et al. [19]. Figs. 3a, 3b, and 3c compare the results to the local fluence rate $G(r)$ predicted using Eq. 12 for biomass concentrations C_X equal to 0.1, 0.45 and 1.0 kg m^{-3}. The tube inner radius r_i was taken as 8 cm, the incident photon flux density q''_{in} in was equal to 500 $\mu mol_{h\nu} m^{-2}\ s^{-1}$, the PAR averaged mass absorption $\overline{A}_{abs}$and scattering $\overline{S}_{sca}$ cross-sections were taken as 160 $m^2\ kg^{-1}$ and 890 $m^2\ kg^{-1}$, respectively, and the PAR-averaged back scattering ratio b was 0.0077.

For the comparison case, Step 6.b of the ray-tracing algorithm was modified such that upon scattering in the culture, a random number was compared to the back scattering ratio b to determine if the ray was scattered into the forward or backward direction rather than using the integrated accumulation function of the Henyey-Greenstein function.

Fig. 3a illustrates poor agreement in the predicted local fluence rate $G(r)$ between the two methods at biomass concentration $C_X = 0.1$ kg m^{-3}. Indeed, the MCRT predicts an extremely large local fluence rate at $r = 0$ as the un-absorbed rays converge at the center point of the tube. This was not the case for the two-flux method which predicted a steady decay in $G(r)$ as r decreased. At $C_X = 0.45$ kg m^{-3}, Fig. 3b illustrates good agreement between the two methods for $r > 1$ cm. However, here too the unabsorbed rays converged at the tube center and the local fluence rate predicted by the MCRT was much larger than that predicted by the two-flux method. At larger biomass concentration, Fig. 3c illustrates a steeper decay in $G(r)$ due to increased absorption by the microalgae cells. Indeed, $G(r)$ decreased to zero for $r > 4$ cm indicating complete light absorption. Here, the strong optical attenuation eliminates the effect of un-absorbed rays convergence at the center point of the tube, and

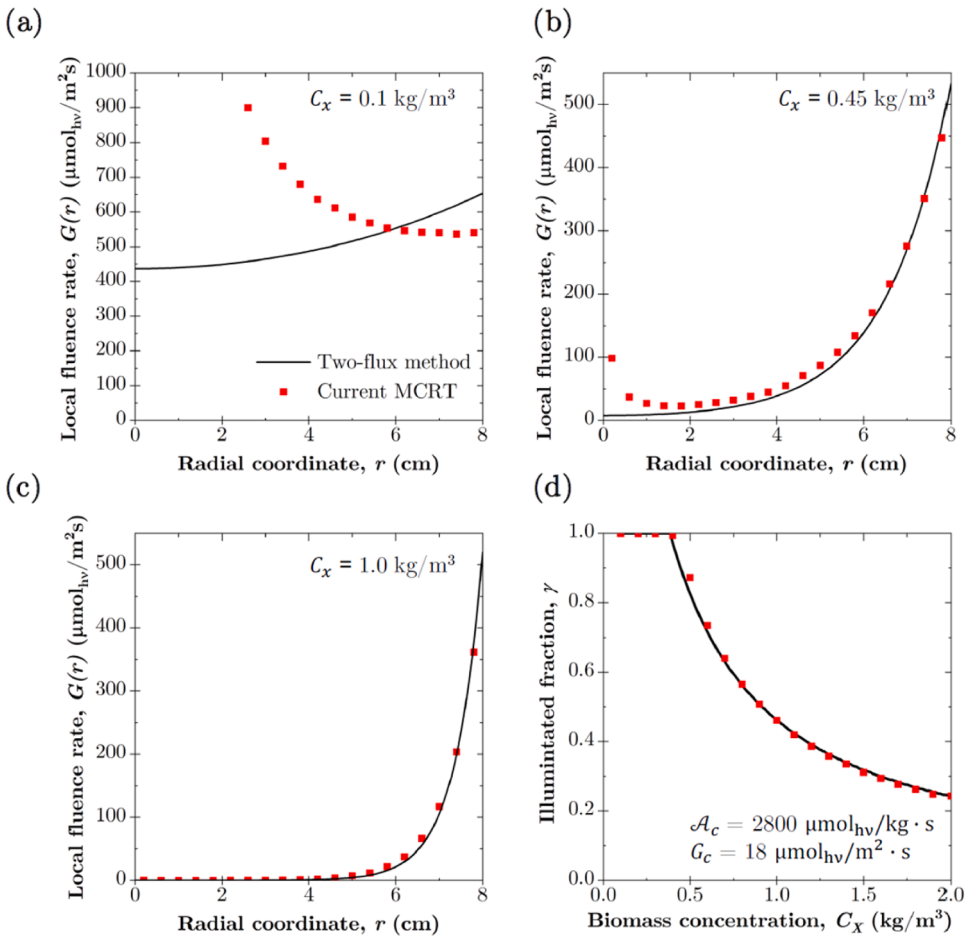

Fig. 3. Comparison of the local fluence rate $G(r)$ (in $\mu mol_{hv} m^{-2} s^{-1}$) predicted using the two-flux method and the current MCRT algorithm for a PBR with an inner radius $r_i = 0.08$ m and biomass concentration C_X of (a) 0.1, (b) 0.45, and (c) 1.0 kg m^{-3} and (d) the corresponding illuminated fraction γ predicted by both methods as a function of biomass concentration.

a good agreement between the two methods was found for all values of tube radius. This suggests that the predictions of $G(r)$ given by the two methods agree when total light absorption occurs (due to the high biomass concentration typically achieved in a PBR, this is the usual mode of operation, as described later), whereas at low biomass concentrations, the MCRT predicts larger $G(r)$ due to the rays converging at the tube center point.

Fig. 3d plots the illuminated fraction γ predicted by both methods as a function of biomass concentration. Here the compensation rate of photon absorption A_c was equal to 2800 $\mu mol_{hv} kg^{-1} s^{-1}$ [11]. Despite the disagreement observed at low biomass concentrations (when the approximation is less accurate) in Figs. 3a,3b and 3d illustrates good agreement in the predicted illuminated fraction γ between the two methods over the range of biomass concentrations considered. This suggests that the MCRT can accurately predict the illuminated fraction γ and local fluence rate $G(r)$ in the case of full light attenuation, i.e., $\gamma < 1$.

3.5. Convergence

Since the Monte-Carlo algorithm is statistical method requiring the sampling of a large number of rays, the confidence interval of the results (that is provided by the standard error of the rays statistics) will depend on the number of ray paths sampled. Moreover, our algorithm is biased by the use of a mesh to discretize the absorption field and calculate the illuminated fraction γ (note that to the date, this bias is unavoidable because no unbiased MCRT approach is available in the literature for evaluating γ). Therefore the results depend on both the number or rays

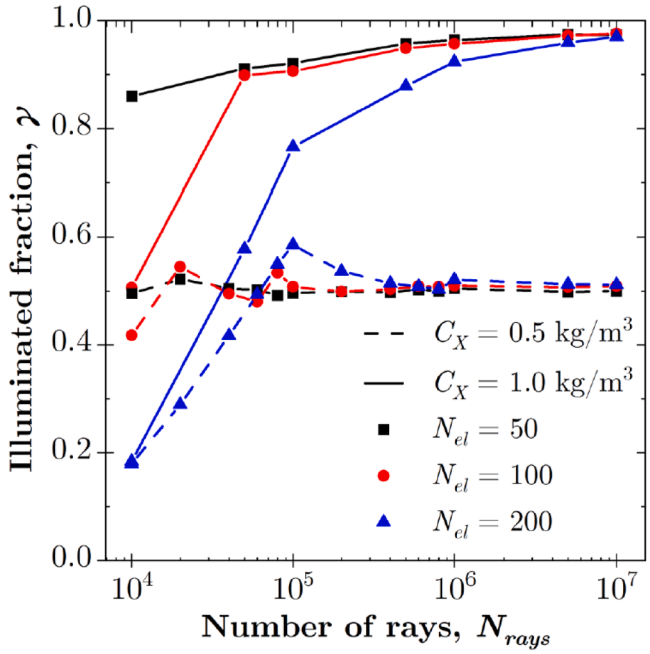

Fig. 4. Predicted illuminated fraction γ using 50, 100, and 200 mesh elements as a function of the number of rays simulated N_{rays} for biomass concentrations of C_X equal to 0.5 and 1.0 kg m^{-3}.

samples and the number of elements in the mesh. Fig. 4 plots the predicted illuminated fraction γ as a function of the number of rays simulated N_{rays} for a number of elements N_{el} equal to 50, 100, and 200 and biomass concentrations equal to 0.5 and 1.0 kg m^{-3}. The microalgae radiative properties $\overline{A}_{abs}$ and $\overline{S}_{sca}$ were equal to 199 m^{2}kg^{-1} and 2873 m^{2}kg^{-1} and were representative of those of *Chlorella vulgaris* for a pigment concentration of 4 wt.%. The photon flux density q''_{in} was composed of collimated, normally incident radiation (i.e., $\theta_{in} = 0°$) and equal to 200 $\mu mol_{h\nu} m^{-2} s^{-1}$. For a given mesh and number of rays N_{rays}, ten trials were performed to assess the standard deviation.

For all values of N_{el} and biomass concentration, the standard deviation in γ was less than 0.005 for N_{rays} greater than 0.5×10^5, corresponding to a 95 % confidence interface of ± 1 %. However, Fig. 4 indicates that despite this, the illuminated fractions γ predicted for different values of N_{el} were not in agreement for a number of rays N_{rays} as low as 0.5×10^5 for a given biomass concentration. Indeed, the predictions given for all values of N_{el} converged for $N_{rays} \geq 0.5\times10^6$ and $N_{rays} \geq 0.5\times10^7$ for biomass concentrations of 0.5 and 1.0 kg m^{-3}, respectively. This indicates that the number of rays N_{rays} required to achieve numerical convergence depended on the conditions within the microalgae culture, i.e., biomass concentration. Thus, for all simulations in the current study, a number of rays N_{rays} was used such that the illuminated fractions γ predicted using N_{el} equal to 100 and 200 were within ± 2 % of the value predicted for $N_{el} = 50$.

4. Results and discussion

4.1. Optical thickness scaling

Fig. 5a plots the predicted illuminated fraction γ within the culture of *Chlorella vulgaris* as a function of biomass concentration C_X for tube inner radius r_i equal to 2, 5, 10, and 20 mm. The photon flux density q''_{in} was composed of collimated, normally incident radiation (i.e., $\theta_{in} = 0°$) and was equal to 200 $\mu mol_{h\nu} m^{-2} s^{-1}$. As already described elsewhere [17, 41], the illuminated fraction γ is an important parameter for describing light conditions in the PBR. A value of $\gamma > 1$ indicates that some light is transmitted, while $\gamma < 1$ indicates that dark volumes occur within the culture, thus productivity is maximized for the "luminostat" regime where $\gamma = 1$. Here, the interest of decreasing the tube diameter is illustrated by the large illuminated fraction γ at relatively large biomass concentrations and low photon flux densities. This was especially the case for a thin tube with an inner radius r_i of 2 mm where ranged from 0.67 to 0.12 for biomass concentrations of 5 and 30 kg m^{-3}, respectively.

Fig. 5b plots the same predicted illuminated fraction γ as a function of the quotient of the biomass concentration and the specific illuminated area of the system, i.e., $C_X / a_{light} = C_X r_i$ representative of the culture optical thickness (also similar to a biomass concentration expressed per unit of illuminated surface, introducing the concept of areal biomass concentration). The results demonstrate a clear scaling relationship between γ and the optical thickness. A parallel can be drawn with other studies that have demonstrated a direct relationship between areal productivity (in g m^{-2} day^{-1}) and optical thickness of a microalgae culture [22]. Our results demonstrate that the scaling behavior is a direct result of the same behavior observed for γ. Thus, despite the complexity of the underlying phenomena involved in light transfer, the results presented in the current study will be valid for any tubular PBR inner radius r_i and culture biomass concentration C_X such that the optical thickness $C_X r_i$ and lighting conditions, i.e., incidence angle, incident diffuse and collimated photon flux, are the same.

4.2. Impact of tube wall thickness

To assess the impact of the tube on the light transfer within the PBR, the flux transmitted through the tube/culture interface q''_{cult} and thus available to the microalgae cells for different tube wall thicknesses t was

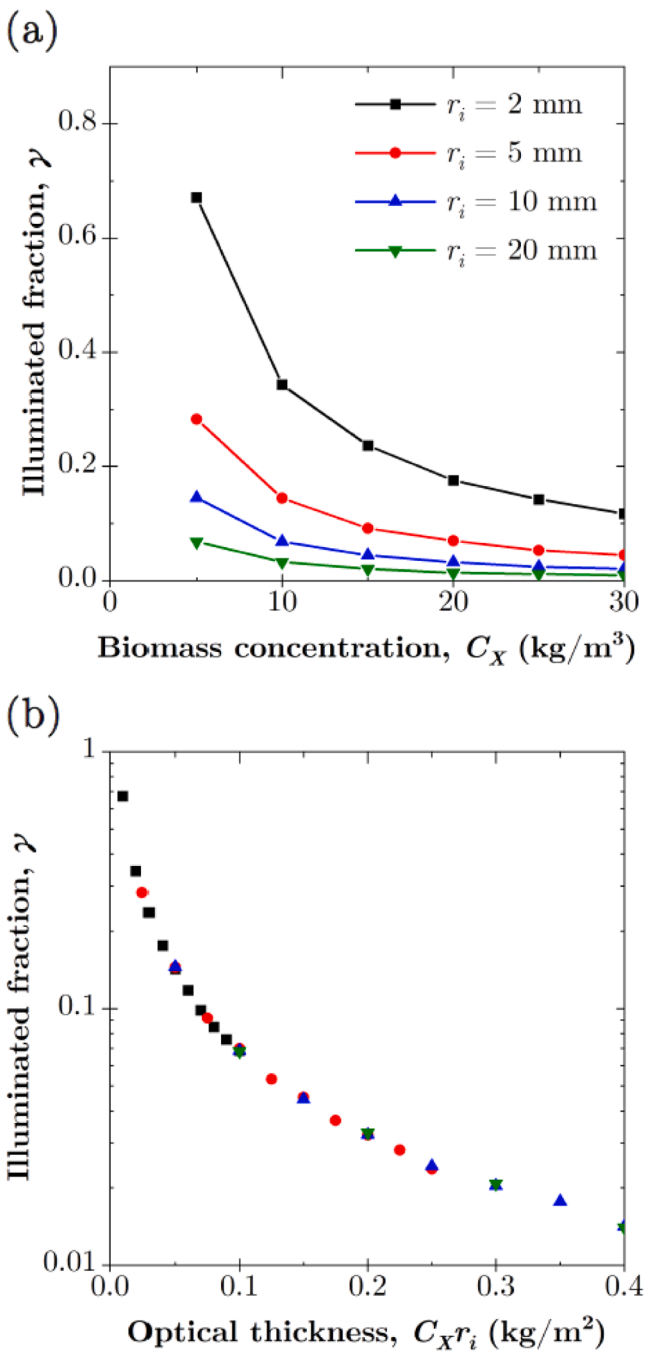

Fig. 5. Predicted illuminated fraction γ for tube inner radius r_i equal to 2, 5, 10, and 20 mm as a function of (a) the biomass concentration C_X and (b) the optical thickness represented by C_X r_i (in kg m^{-2}) for a photon flux density q''_{in} = 200 $\mu mol_{h\nu} m^{-2} s^{-1}$.

considered. The photon flux available to the culture q''_{cult} was calculated using the MCRT algorithm by terminating a given ray once it was transmitted through the tube/culture interface. Then q''_{cult} was taken as

$$q''_{cult} = \frac{E_{ray} N_{cult}}{\pi r_i h} \tag{14}$$

where N_{cult} is the number of rays transmitted through the tube/culture interface and available to the culture for absorption. To generalize the results, the ratio q''_{cult}/q''_{in} was considered as a function of the normalized tube wall thickness, i.e., t/r_o. Note that the ratio q''_{cult}/q''_{in} is only a function of the tube geometry and is independent of the radiative

properties of the microalgae cells, i.e. $\overline{A}_{abs}$, $\overline{S}_{sca}$, g, and the operational parameters of the PBR, i.e., C_X, q''_{in}. Thus, the normalized tube wall thickness t/r_o can be considered a design parameter for tubular PBRs.

Fig. 6a plots the ratio q''_{cult}/q''_{in} for normalized tube wall thicknesses t/r_o ranging from 0.01 to 0.9 and for a collimated photon flux with incidence angle θ_{in} ranging from 0° (i.e., normal incidence) to 80° Similarly, Fig. 6b plots q''_{cult}/q''_{in} as a function of t/r_o for the case of diffuse incidence. For collimated incidence, Fig. 6a indicates that the ratio q''_{cult}/q''_{in} increased with increasing tube wall thickness. In fact, for all incidence angles considered, q''_{cult}/q''_{in} exceeded unity for large values of normalized tube wall thickness. This indicates that the photon flux available to the culture was larger than photon flux incident on the PBR external surface, i.e., $q''_{cult} > q''_{in}$. Indeed, as tube wall thickness increased, the area of the tube increased and more light was intercepted by the PBR. This additional light was then refracted at the air/tube interface towards the tube/culture interface creating a concentrating effect and resulting in $q''_{cult}/q''_{in} > 1$. This suggests that a large tube wall thickness t relative to the outer radius r_i of the PBR may increase the microalgae growth rate by increasing the photon flux available to the microalgae cells. For diffuse incidence, Fig. 6b indicates that a concentrating effect was observed for $t/r_o > 0.2$, however, it was significantly less pronounced than the direct incidence case since only a small fraction of rays were incident at a direction that would result in them being refracted towards the culture.

For lower incidence angles $\theta_{in}$of 0°, 20°, and 40°, q''_{cult}/q''_{in} increased with increased t/r_o until it reached a plateau of 1.25, 1.29, and 1.42, respectively. Once this plateau was reached, increasing the tube wall thickness did not increase q''_{cult}/q''_{in} since the additional rays captured were not incident on the tube/culture interface. For incidence angles $\theta_{in} > 40°$, q''_{cult}/q''_{in} increased monotonically with increasing normalized tube wall thickness t/r_o. For tube wall thickness $t/r_o \geq 0.5$, q''_{cult}/q''_{in}increased with increasing incidence angle θ_{in} (with the exception of θ_{in}= 80°). Figs. 6c and 6d show the path of rays refracted at the air/tube boundary for $t/r_o = 0.6$ and incidence angle θ_{in} equal to 0° and 60° These figures demonstrate the increased concentrating effect at larger incidence angles θ_{in}. As θ_{in} increased, the focal point of refracted rays shifted closer to the tube center, increasing the intensity of the light flux on the microalgae culture.

Fig. 7a plots the predicted illuminated fraction γ as a function of tube wall thickness t for tube inner radius of r_i equal to 2, 4, and 6 mm and incidence angle θ_{in} equal to 0° and 45° for an incident photon flux density $q''_{in} = 200\ \mu mol_h m^{-2} s^{-1}$. To isolate the impact of the tube wall thickness, the biomass concentration was taken such that $C_X r_i$ was equal to 0.01 kg m^{-2} for each inner radius r_i simulated. The results indicate that the illuminated fraction increased to a maximum value with increasing tube wall thickness t for both incidence angles θ_{in} and all inner radii r_i considered. This can be explained by the concentrating effect observed in Fig. 6a for thicker tube walls which sent more light to

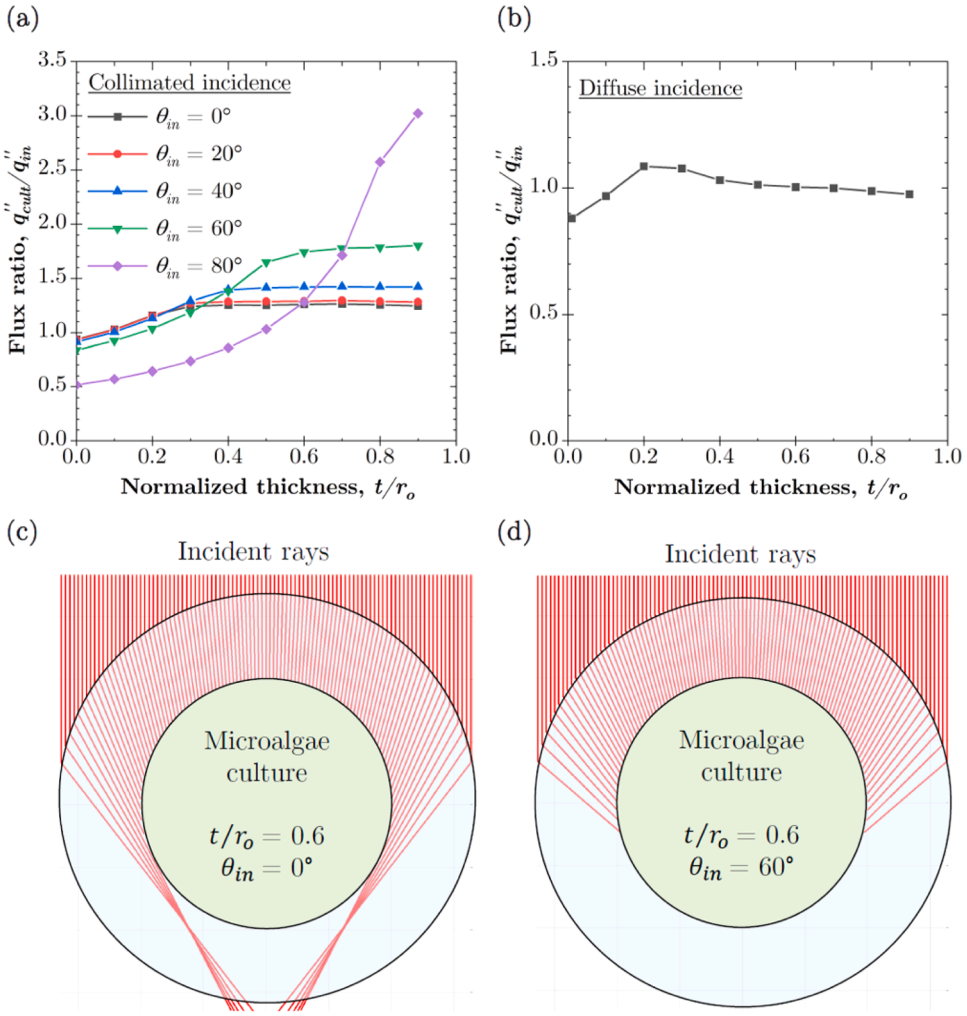

Fig. 6. Flux ratio q''_{cult}/q''_{in} as a function of normalized tube wall thickness t/r_o for (a) collimated radiation with incidence angle θ_{in} ranging from 0° to 80° and (b) diffuse radiation and (c,d) schematic representations of the paths of refracted rays for collimated radiation and normalized tube wall thickness $t/r_o = 0.6$ for $\theta_{in} =$ 0°and 60°, respectively.

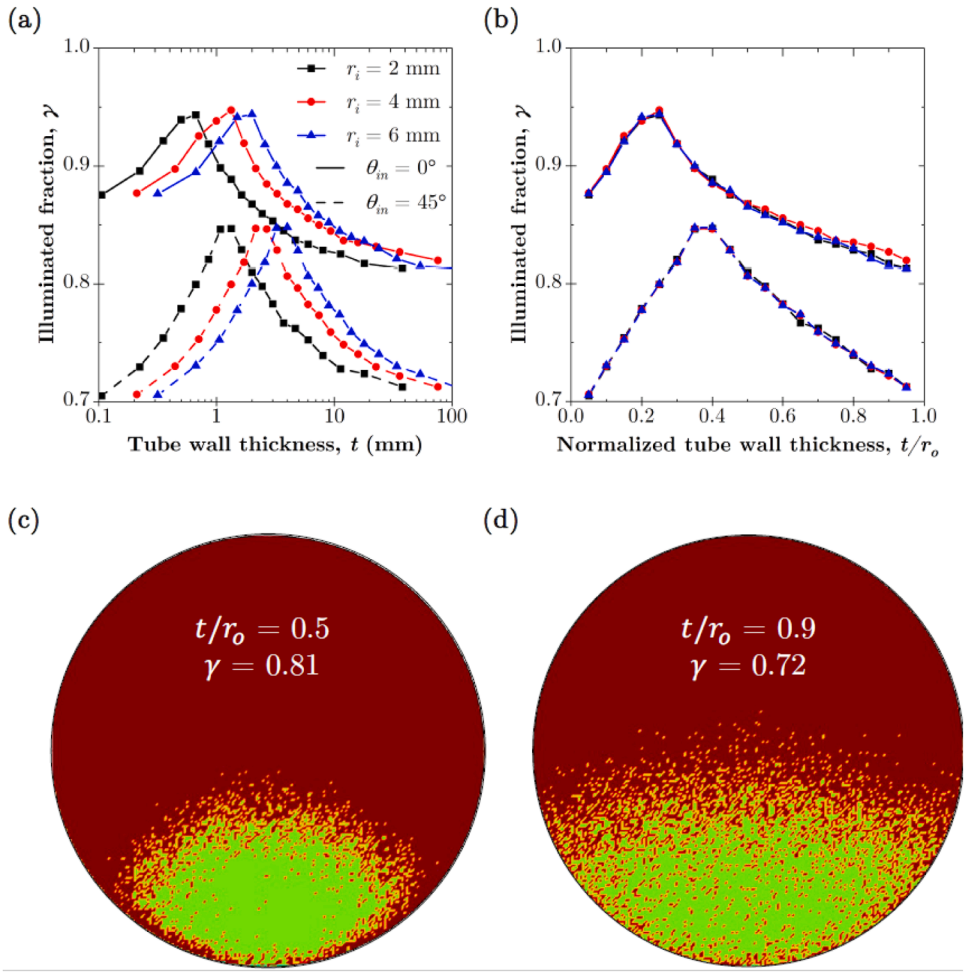

Fig. 7. Illuminated fraction γ as a function of (a) tube wall thickness for tube inner radii r_i equal to 2, 4, and 6 mm and (b) normalized tube wall thickness t/r_o for incidence angles θ_{in} of 0° and 45° (c,d) Map of culture locations where the local rate of photon absorption exceed the compensation rate of photon absorption A(x, y) > A_c for θ_{in} = 45°and t/r_o equal to 0.5 and 0.9, respectively.

the microalgae culture, increasing the light penetration depth and the illuminated fraction γ. Fig. 7a also indicates that γ was smaller for an incidence angle θ_{in} equal to 45° This was attributed to an increase in the reflectance at the air/tube interface and a decrease in the total energy incident upon the PBR in the case of non-normal incidence.

Figs. 7a and 7b demonstrate that t/r_o is a useful parameter than can be adjusted to increase γ (and so to reduce dark volumes in culture volume). Nonetheless, for the cases plotted, adjusting t/r_o was not sufficient to reach the ideal condition $\gamma = 1$ (i.e. full light absorption but no dark volume). Instead, other parameters such as optical thickness $C_X r_i$ and/or incident photon flux q''_{in}would also have to be adjusted to approach $\gamma = 1$ (see later for a detailed investigation). However, as also mentioned by [23], in contrary to PBR presenting flat surfaces (flat panel PBR, open ponds), achieving optimal light attenuation conditions (as represented by $\gamma = 1$ condition and also maximal growth rate) will be not possible in tubular geometries because of the refraction at the air-liquid curved interface which lead to a light concentrating effect in the culture volume.

Fig. 7b plots the predicted illuminated fraction γ as a function of the normalized tube wall thickness t/r_o. Interestingly, the results for all inner radii r_i collapse unto the same curve for both incidence angles. Note this result was also observed for diffuse incidence (results not shown). For the current value of $C_X r_i = 0.01$ kg m^{-2}, the optimum normalized tube wall thickness was 0.25 and 0.4 for θ_{in} equal to 0° and 45°, respectively. Fig. 7b indicates that γ decreased steadily with increasing t/r_o for both incidence angles. This was the case despite the fact that the ratio q''_{cult}/q''_{in} increased and then plateaued for values of t/r_o beyond the optimum values identified here. This can be explained by the distribution of light absorption between t/r_o equal to 0.5 compared to 0.9. This is illustrated in Figs. 7c and 7d, respectively, which show the areas where the LRPA was greater than the compensation LRPA, i.e., A (x, y) > A_c, in red and the areas where A (x, y) < A_c in green for $\theta_{in} = 45°$ Notably, at $t/r_o = 0.5$, Fig. 7c indicates that the culture was illuminated from the sides as well as the front due to the refractive index mismatch between the air and tube walls causing light to be refracted towards the inner cylinder (see Fig. 6c and 6d). However, for $t/r_o = 0.9$, Fig. 7d indicates that only the front half of the culture was illuminated. Indeed, as t/r_o increased, the radius r_i decreased relative to the outer radius r_o and the refraction effects of the tube wall were less important.

4.3. Impact of incidence angle

Tubular PBRs under solar conditions can experience the whole range of possible incidence angles, i.e., θ_{in} from 0 to 90° [42] (simulations with a time-varying angle of incidence will be presented in section 3.8, where growth simulations will be performed on typical days of the year). Thus, Fig. 8 plots the predicted illuminated fraction γ for the case of collimated incident radiation as a function of incidence angle θ_{in} for normalized tube wall thickness t/r_o equal to 0.01, 0.30, and 0.50, for an optical thickness $C_X r_i = 0.02$ kg m^{-2} an for the same photon flux density q''_{in} = 200 $\mu mol_{hv} m^{-2} s^{-1}$. Here, the illuminated fraction decreased monotonically with increasing incidence angle θ_{in} for all three values of t/r_o.

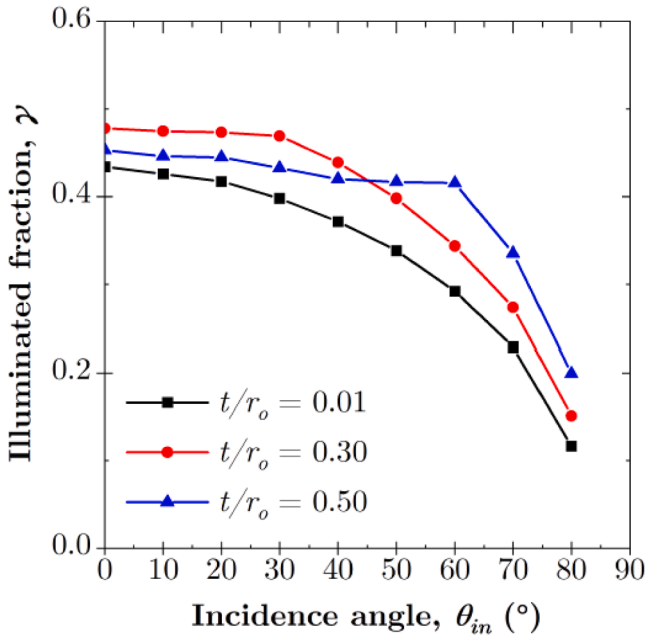

Fig. 8. Predicted illuminated fraction γ for collimated incident radiation as a function of incidence angles θ_{in} for normalized tube wall thickness t/r_o equal to 0.01, 0.3 and 0.5 respectively.

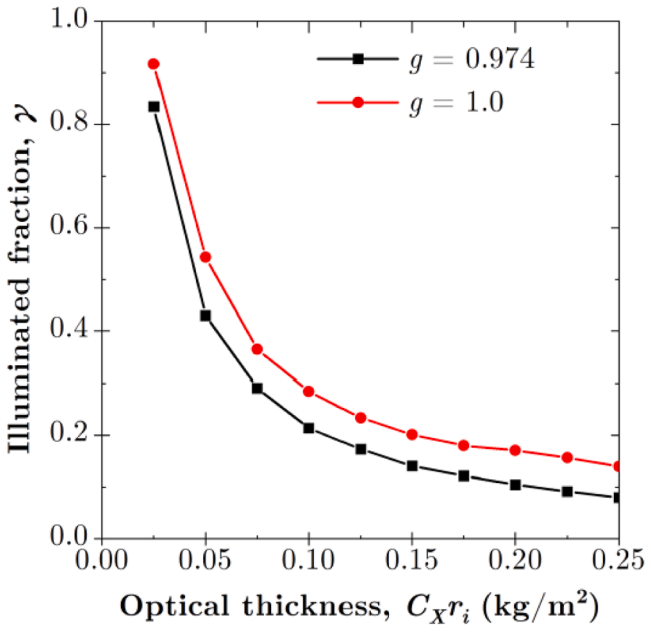

Fig. 9. Illumined fraction γ as a function of biomass concentration for a microalgae cell asymmetry factor g equal to 0.974 and 1.0 representative of negligible scattering.

This was due to increased reflection at the air/tube interface as the incidence angle increased. For incidence angles $\theta_{in} < 40°$ the illuminated fraction was largest for $t/r_o = 0.30$. This was thanks to the larger concentrating effect of the thicker tube walls compared to $t/r_o = 0.01$ and the refraction at the air/tube interface which illuminated the front and sides of the culture as observed in Fig. 7c. However, for incidence angles $\theta_{in} > 40°$, the illuminated fraction γ was largest for $t/r_o = 0.50$. This was due to the concentrating effect observed in Fig. 6d which moved the focal point of the refracted rays towards the tube center of the tube as the incidence angle increased.

4.4. Impact of scattering

Fig. 9 plots the illuminated fraction γ as a function of the optical thickness $C_X r_i$ for the case of an asymmetry factor g equal to unity, i.e., negligible scattering by the microalgae, and for the case of an asymmetry factor g equal to 0.974 as reported in the literature for *Chlorella vulgaris* [26]. The photon flux density q''_{in} was composed of collimated, normally incident radiation (i.e., $\theta_{in} = 0°$) and was equal to 200 $\mu mol_{h\nu} m^{-2} s^{-1}$. For both cases, the illuminated fraction γ decreased exponentially with increasing biomass concentration (see Fig. 5). However, Fig. 9 indicates that γ was larger when scattering by the microalgae was neglected, i.e., $g = 1.0$, than when it was accounted for with an asymmetry factor of $g = 0.974$. Interestingly, this was the case despite the fact that an asymmetry factor g of 0.974, representing a strongly forward-scattering particle, is only slightly different than an asymmetry factor $g = 1.0$, representing a perfectly forward-scattering particle. This can be explained by the large mass scattering cross-section of microalgae relative to the absorption cross-section, which resulted in a large single-scattering albedo ω. Thus, photons could deviate significantly from the forward direction due to the many scattering events that took place before a photon was absorbed. Our results show that assuming negligible scattering by the microalgae could cause the illuminated fraction γ to be over estimated by 25 % at low biomass concentrations where γ was the largest. Then, scattering should not be neglected for light transfer modeling in tubular PBRs, as has been done previously [23].

Fig. 10a plots the local fluence rate normalized with respect to the incident photon flux $G(x,y)/q''_{in}$ for an microalgae asymmetry factor g equal to 1 and 0.974 and optical thickness $C_X r_i$ of 0.05 kg m^{-2}. Fig. 10b plots the area where the LRPA was greater than that of the compensation LRPA, i.e., A $(x,y) >$ A $_c$. For the case of $g = 1.0$, the incident light was scattered in the forward direction and therefore penetrated deeper into the microalgae culture. This phenomenon explains the larger values of illuminated fraction achieved for the culture with negligible scattering. On the other hand, for $g = 0.974$, larger normalized local fluence rate $G(x,y)/q''_{in}$ near the culture surface indicated that scattering by the algae caused light to be absorbed closer to the culture surface. Finally, Fig.11b indicates that lines of larger $G(x,y)/q''_{in}$ were present in the lower half of the tube when scattering was neglected. However, these rays were not present for $g = 0.974$. This suggests that, unlike flat-panel PBRs [15,43], the local fluence rate $G(x,y)$ is highly sensitive to the microalgae asymmetry factor g in tubular PBRs.

4.5. Influence on volumetric and areal growth rate

Fig. 11 plots evolutions of illuminated light fraction γ (Fig. 11-a), predicted average volumetric growth rate $\langle r_X \rangle$ (in kg m^{-3} day^{-1}) (Fig. 11-b)) and areal average volumetric growth rate $\langle r_S \rangle$ (in g m^{-2} day^{-1}) (Fig. 11-c) as a function of normalized tube wall thickness t/r_o, for different values of inner tube radius r_i ranging from 0.005 m to 0.02 m and for incidence angle θ_{in} equal to 0° and 45° As in previous cases, the incident PFD was 200 $\mu mol_{h\nu} m^{-2} s^{-1}$ and the biomass concentration $C_X r_i$ was equal to 0.01 kg m^{-2} for each inner radius r_i simulated. Simulations were also conducted for diffuse incidence, with an incident PFD q''_{in} = 200 $\mu mol_{h\nu} m^{-2} s^{-1}$ (Fig. 11-b-d-f).

The volumetric growth rate $\langle r_X \rangle$ is found to increase when decreasing the inner tube radius r_i. This is a well-known result, volumetric kinetic performances of any light-limited PBR being fully dependent of culture depth [10]. In our case, decreasing the inner radius r_i from 0.02 m to 0.005 m increases the volumetric biomass productivity by a factor of around 5, emphasizing the interest of decreasing the depth of culture for volumetric performances intensification. The results indicate that the illuminated fraction increased to a maximum value with increasing normal tube wall thickness t/r_o for both direct and diffuse light, both incidence angles θ_{in} and all inner radii r_i considered. This can be

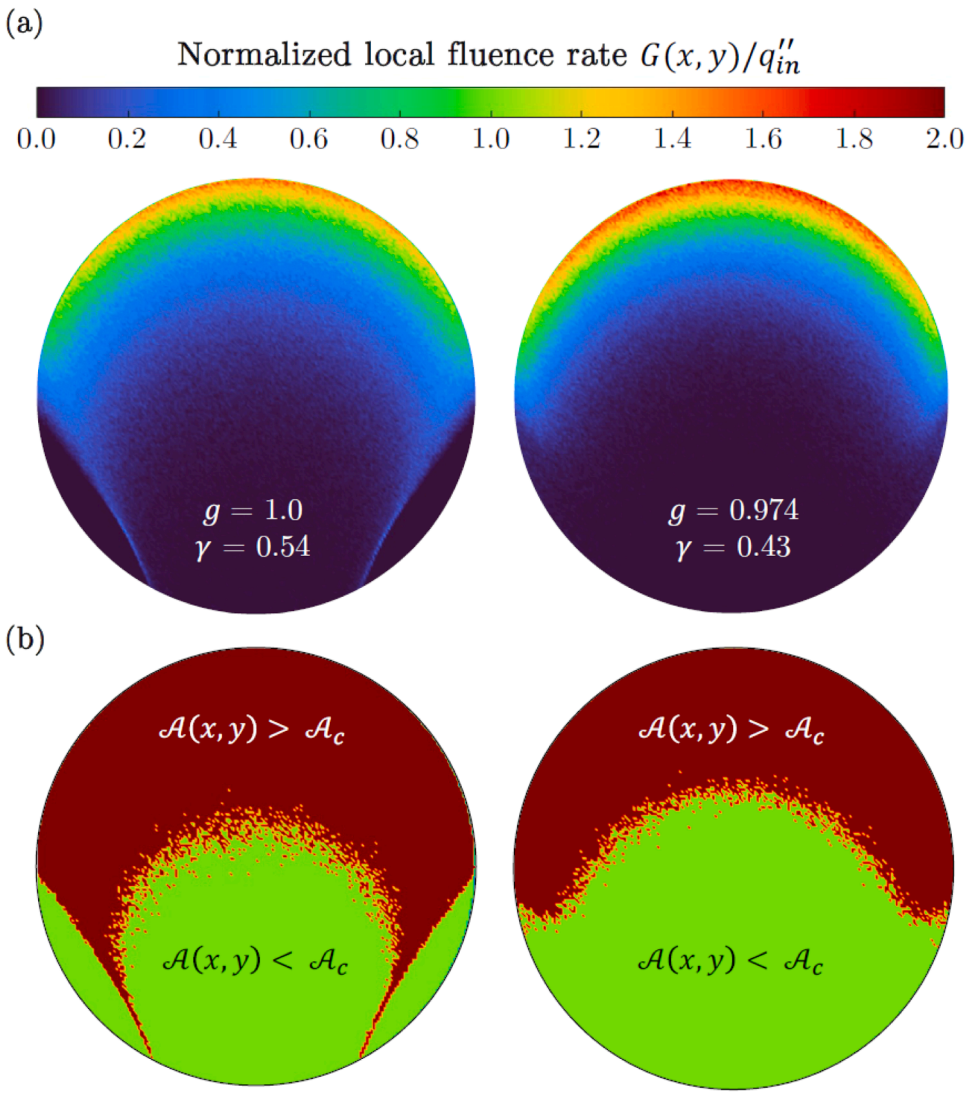

Fig. 10. (a) Normalized local fluence rate $G(x,y)/q''_{in}$ for the case of $g = 1$ (i.e., negligible scattering) and $g = 0.974$ and (b) corresponding culture locations where the LRPA was greater than the compensation LRPA, i.e., A(x, y) > A_c(red area) and less than the compensation LRPA, i.e., A(x, y) < A_c (yellow).

explained by the concentrating effect observed in Fig. 6a. We can note that in all cases, the illumination fraction remains below 1, indicating that full light absorption occurs in the culture volume but with the presence of a dark volume where the LRPA was smaller than the compensation LRPA, i.e., A (x, y) < A $_c$.

Interestingly, the concentrating effect also corresponds in an increase in growth rate $\langle r_X \rangle$ up to an optimal value of the normalized tube wall thickness t/r_o for each incidence angle, namely t/r_o around 0.2 and 0.4 for normal and 45° incidence respectively. A similar trend is observed for diffuse incidence but with a less marked effect as soon as the normalized tube wall thickness t/r_o is larger than 0.2. Moreover, we note that the maximum value of γ and $\langle r_X \rangle$ occurred at the same tube wall thickness t/r_o for a given incidence angle (Fig. 11-a), emphasizing the direct relation between illuminated light fraction γ and resulting biomass productivity $\langle r_X \rangle$, as already observed elsewhere [19,36,44]. These results suggest that the biomass growth rate can be improved by optimizing the tube wall thickness. Indeed, for $\theta_{in} = 45°$, increasing t/r_o from 0.05 to 0.4 resulted in an increase in the predicted average growth rate of 0.9 kg m^{-3}day^{-1} for r_i=0.005 m which represents a 60 % increase in growth. Similar results were observed for diffuse incidence where increasing t/r_o from 0.1 to 0.2 resulted in an increase of 0.4 kg m^{-3}day^{-1} or 15 % for the same inner radius value.

In an attempt to provide more general guidelines for tubular PBR design optimization, Fig. 11-e (collimated light) and 11-f (diffuse light) presents the average areal growth rate ($\langle r_S \rangle$ in g m^{-2}day^{-1}). The average areal growth rate was determined from the specific illuminated surface $a_{light} = \frac{S_{light}}{V_{cul}}$ [10]:

$$\langle r_S \rangle = \langle r_X \rangle \frac{V_{cul}}{S_{light}} = \frac{\langle r_X \rangle}{a_{light}} \tag{15}$$

where V_{cul} is the culture volume and S_{light} is the illuminated surface. Note that in the configuration of a tubular PBR, the illuminated surface can be defined with respect to the inner and outer tube radius (this will be discussed in more details in next section). Here the inner radius will be used as a reference (i.e. surface of culture illuminated), with then:

$$a_{light} = \frac{S_{light}}{V_{cul}} = \frac{\pi r_i H}{\pi r_i^2 H} = \frac{1}{r_i} \tag{16}$$

As observed for the illuminated fraction, when using areal growth rate, the results for all inner radii r_i collapse unto the same curve for both incidence angles. The same is observed for diffuse light. The relevance of using area-based values for their genericity in the comparison of various culture system performances is well-known [44]. This is here confirmed, despite the very underlying complex phenomena involved in the light transfer in tubular PBRs. When combined to other parameters previously

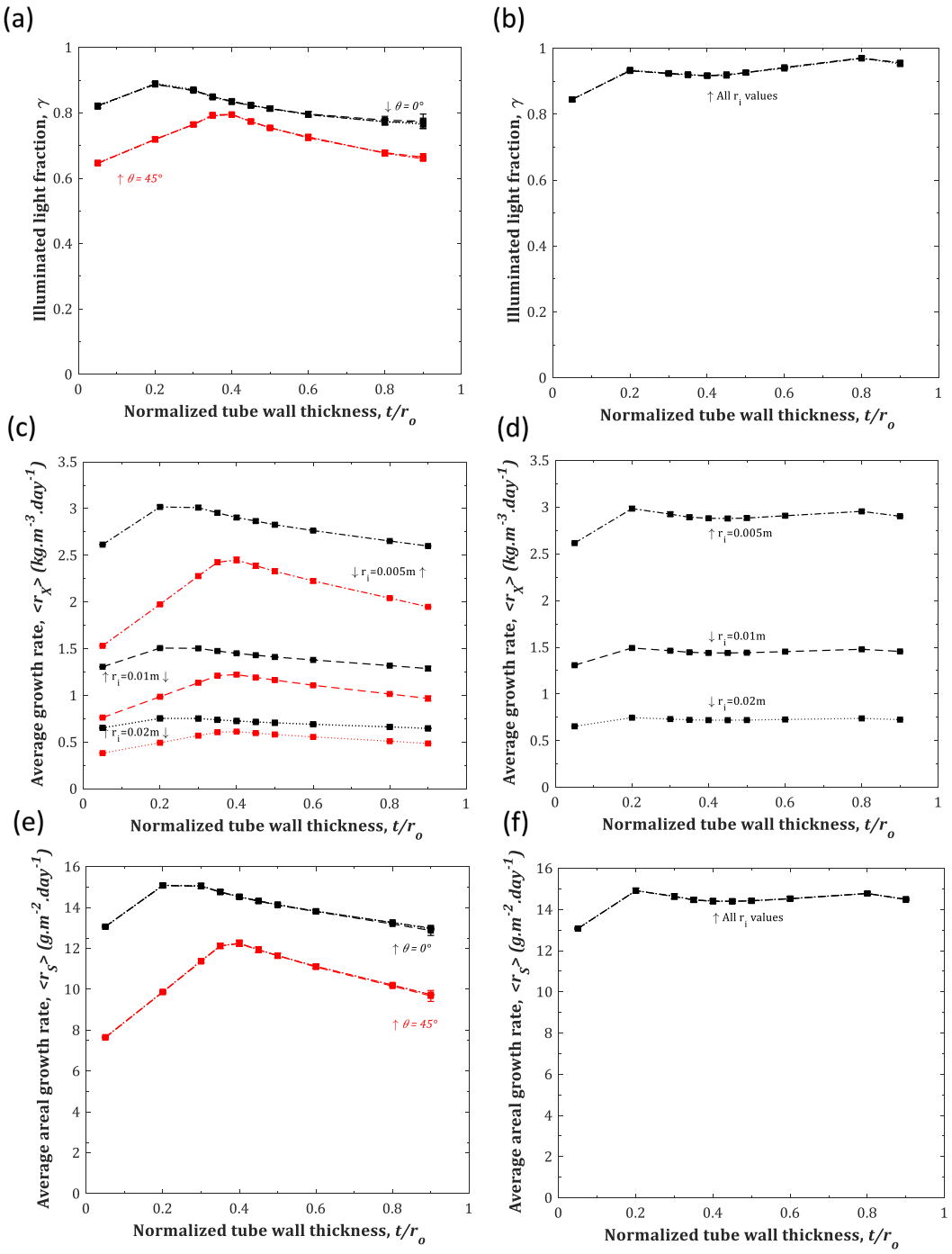

Fig. 11. Predicted illuminated fraction γ (a-b), average volumetric growth rate $<r_X>$ (c-d) and average areal growth rate $\langle r_S \rangle$ (e-f) as a function of normalized tube wall thickness t/r_o for collimated incidence with incidence angles θ_{in} equal to 0° and 45° (a-c-e) and diffuse incidence (b-d-f).

discussed such as the illuminated light fraction (which also collapse for all r_i values) and the relevance of optical thickness $C_X\ r_i$ (in kg m^{-2}, which value could guide tube diameter selection) and normalized tube thickness t/r_o as scaling parameters, areal biomass productivity $\langle r_S \rangle$ can reveal useful to define generic approaches for tubular PBR design, optimization and performance prediction.

In addition to demonstrating the interest of areal biomass concentration, areal biomass productivity and normalized tube thickness as scaling parameters, our results allow defining general guidelines for tubular PBR optimization:

- The inner diameter r_i (and then $a_{light} = 1/r_i$) was confirmed as the main engineering parameter for volumetric performances intensification (i.e. volumetric growth rate but also biomass concentration, both being directly related).
- For appropriate values, the outer radius r_o was found relevant to induce a light concentrating effect, with a possible additional improvement in productivities (both volumetric and areal productivities). Optimal values were found dependent of the incident angle, but normalized tube wall thickness t/r_o in optimal values were found in the range of 0.2 to 0.4 for all values of inner radius. For a tube wall thickness of between 0.003 and 0.005 m, as is generally

observed in practice, this leads to a maximum tube inside diameter of about 0.016 m.

– In all cases, and as already observed for flat panel geometries [11, 36], increasing the incident angle was found to reduce productivities, with a direct relation to illuminated light fraction which was also found to decrease with increasing incident angle.

4.6. Comparison with flat panel PBRs

Fig. 12 illustrates the interest of using normalized tube wall thickness and average areal growth rate to compare different PBRs geometries. Here the comparison is made between a tubular PBR with inner radius r_i=0.03 m, corresponding to a tubular PBR commercialized by LgeM company (Lgem, the Netherlands), and a flat panel PBR of depth L with a glass wall of the same thickness and optical properties as the tube wall. For a representative comparison, similar specific illuminated ratio were applied for both geometries, with then a_{light} =1/r_i=1/L. The optical thickness based on culture depth L was also the same for both flat panel and tubular reactors, i.e., $C_X / a_{light} = C_X L = 0.01$ kg m^{-2}. Same incident photons flux density was applied in both cases for both direct and diffuse radiation (q''_{in} =200 μmol$_{h\nu}$m^{-2}s^{-1}). Note however that because of the difference in illuminated surface geometry, the photons flux density averaged on the PBR optical surface was different for the flat panel PBR ($q''_{in} = I_{col}cos(\theta_{in}) + \pi I_{dif} = q''_{\perp}cos(\theta_{in}) + q''_{\cap}$) than for the tubular PBR ($q''_{in} = (2/\pi)I_{col}cos(\theta_{in}) + \pi I_{dif} = (2/\pi)q''_{\perp}cos(\theta_{in}) + q''_{\cap}$) due to presence of curved tube walls (see Appendice).

Fig. 12-a presents prediction of areal growth rate $\langle r_S \rangle$ and illuminated light fraction γ (Fig. 12-c) as a function of normalized tube wall thickness. For a flat panel reactor, the predicted areal growth rate was found independent of the wall thickness since the glass was considered to be non-absorbing and because of the absence of curvature. Furthermore, unlike tubular reactors, flat panel PBRs did not exhibit a concentrating effect (i.e. plane optical surfaces), thus the photon flux delivered to the culture was similar for all wall thicknesses. The areal growth rate $\langle r_S \rangle$ was found lower in tubular PBR than with flat panel PBR for normal incidence. Increasing the normalized tube wall thickness in the range 0.2–0.3 results in an improvement of the growth rate for the tubular PBR, leading to similar values for both geometries. For 45° incident angle, optimizing the normalized tube wall thickness was found more relevant, with larger areal growth rate for the tubular PBR for normalized tube wall thickness in the range 0.25–0.6. For diffuse light, tubular PBR leads to larger values of areal growth rate and for a large range of tube wall thickness. Curved geometries allows to increase the amount of diffuse light collected onto the illuminated surface (by π/2 for a given photons flux density $q''_{\cap}$, see Appendice) and are less sensitive to diffuse incidence. As shown in Pruvost et al. [42], PBR presenting flat surfaces (flat panel PBR, raceways…) are indeed highly sensitive to the incident angle, which influences light received onto the surface (i.e. decreased by cosθ_{in}) but also reduces light penetration in the culture depth due to oblique incidence. Therefore, diffuse light (covering then the all range of incident angles) has a more negative influence in the case of flat panel PBR.

Fig. 12-c shows that illuminated fraction γ was always lower than 1 for the tubular PBR, in contrary to the flat panel PBR where the ideal condition of γ=1 was obtained for normal incidence. This is in agreement with our previous statement on the difficulty to reach γ=1 condition in tubular PBRs because of light refraction into the tube wall (see discussion on Fig. 4). The influence on resulting growth rate will be explained in more details hereafter (Fig. 13).

From a practical point of view, increasing the tube wall thickness to induce a concentrating light effect also leads to an increase in the area covered by the tube and so the PBR footprint for a given culture volume. To illustrate this, the outer tube radius can be used as a reference in the definition of the specific illuminated surface:

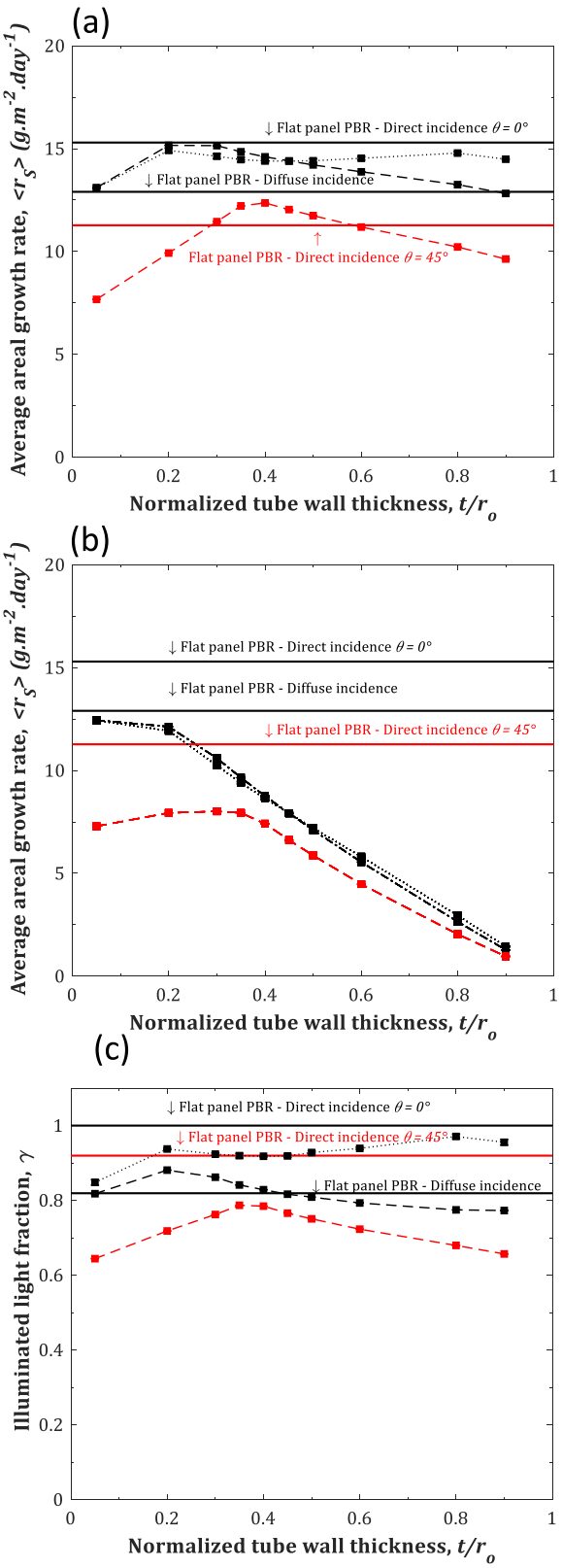

Fig. 12. Comparison between flat panel and tubular PBRs. Predicted average areal growth rate $\langle r_s \rangle$ using a_{light} as a reference (a), average areal growth rate $\langle r_S \rangle$ using $a_{light,outer}$ as reference (b) and illuminated fraction γ (c), as a function of normalized tube wall thickness t/r_o for $_{in}$ equal to 0° (black dashed line) and 45° (red dashed line) and diffuse incidence (black dotted line). Predictions for flat panel PBR are in solid lines.

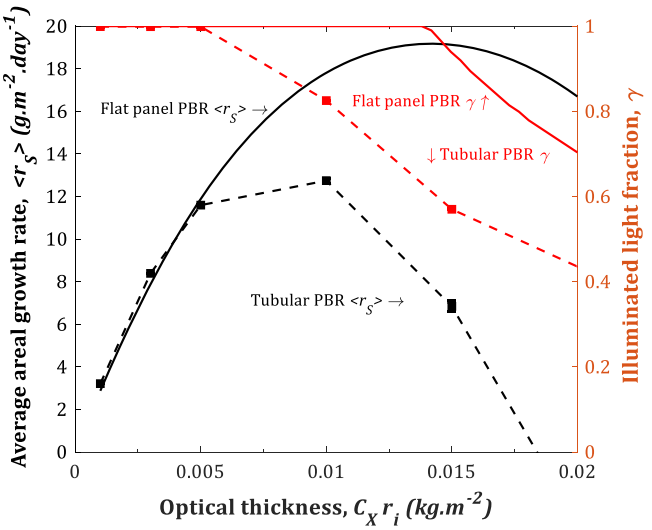

Fig. 13. Prediction of average areal growth rate $\langle r_S \rangle$ (black lines) and illuminated light fraction γ (red lines) as a function of optical thickness $C_X\, r_i$ (in kg m^{-2}) for tubular (dashed lines) and flat panel (solid lines) PBRs.

$$a_{light,\ outer} = \frac{S_{light,\ outer}}{V_{culture}} = \frac{\pi r_o H}{\pi r_i^2 H} = \frac{r_o}{r_i^2} \tag{17}$$

Fig. 12-b presents evolution of the areal growth rate when using such definition in Eq.15. The negative effect of applying large values of tube wall thickness because of the resulting increase in PBR size for given culture volume is here clearly illustrated. For small values of tube wall thickness, the concentrating light effect tends to compensate the increase of tube size by increasing the area for light interception then refracted toward the culture volume (especially in the case of diffuse light, as explained before). But the efficiency decreases progressively because of the increase of photons deviated but not collected by the culture (Fig. 6). For very large values of tube wall thickness, very low areal growth rate are obtained (when considering the outer tube surface - and then PBR footprint - as a reference).

A comparison can be made with the tubular PBR marketed by the company Lgem and used as a case study. The outer radius is r_o= 0.0325 m corresponding to a wall thickness and normalized wall thickness of t = 0.0025 m and t/r_o = 0.077 respectively. The light concentrating effect can then be considered moderate (increase in productivity of about 10 to 20 % depending on the angle of incidence – Fig. 12-a) but sufficient to compensate for the increase in surface area due to the thickness of the tube (compared to a hypothetical zero tube thickness – Fig. 12-b).

4.7. Effect of optical thickness on light transfer conditions and resulting growth rate in tubular and flat panel PBRs

For a better understanding of the difference observed between tubular and flat panel PBR, the effect of biomass concentration (here expressed in terms of optical thickness $C_X\, r_i$) on both illuminated light fraction and average areal growth rate was investigated. The aim was here to emphasize the direct coupling between light attenuation conditions in the culture volume (as a result of optical thickness) and resulting growth rates. Results are given in Fig. 13 for normal incidence and collimated light with q''_{in} = 200 $\mu mol_{h\nu} m^{-2} s^{-1}$ (same conclusion for diffuse light and other incident angles). A normalized tube wall thickness of 0.3 was here applied to maximize the light concentrating effect.

As already demonstrated in several works [19,44,45], maximal areal growth rate was obtained for an optimal value of biomass concentration (i.e. optical thickness), also corresponding to the condition of illuminated light fraction $\gamma = 1$. For the flat panel PBR, this corresponds to a value of optical thickness of 0.013 $kg.m^{-2}$. For the tubular PBR, maximum areal growth rate was obtained for an optical thickness of around 0.01 $kg.m^{-2}$ (confirming then the choice of the value used in previous simulations). But interestingly, this corresponds to an illuminated light fraction γ of 0.8, with then 20 % of dark volume in the culture volume. The condition of $\gamma = 1$ was then obtained, but with lower areal growth rate. This result emphasizes that achieving optimal light attenuation conditions, as represented by $\gamma = 1$ condition and also maximal growth rate, cannot be achieved in tubular PBRs because of the refraction at the air-liquid curved interface which leads to more complex and heterogeneous radiation field. So, even if the condition of $\gamma = 1$ could be reached, this is also obtained at a lower optical thickness than the optimal one leading to maximal growth rate. Indeed, for all values of optical thickness larger than 0.005 $kg.m^{-2}$, a higher areal growth rate was obtained for flat panel PBR, while for lower values, areal growth rate were found similar. A direct relation is here again emphasized with the illuminated light fraction which allows explaining such behavior. Because of the more complex phenomena involved in the light transfer in tubular PBRs, dark volumes appeared in the culture volume even for low values of optical thickness, leading then to a lower efficiency in photosynthetic conversion onto the culture volume. As a result, when applying the optical thickness of 0.013 $kg.m^{-2}$, which was optimal for flat panel PBR ($\gamma = 1$), a dark volume of around 40 % was obtained in tubular PBRs (γ of 0.6). But for a lower optical thickness than 0.005 kg. m^{-2}, although $\gamma = 1$ condition was obtained in tubular PBR, a lower average growth rate was obtained. This is explained by incomplete light absorption in the culture volume (i.e. a part of light received onto the culture is transmitted), and also because of the light concentrating effect which resulted in larger values of LRPA, and then lower local values of photosynthetic conversion efficiency.

Note that because of the use of optical thickness, areal growth rate and normalized tube wall thickness, all results and conclusions presented in this section are valid for any value of inner and outer radius of tubular PBR as well as depth of flat panel PBR. Note also that volumetric performances can be obtained easily from Eq.15.

4.8. Solar modeling

To illustrate the complex interaction between the inclination angle of the tubular PBR and its orientation relative to the sun, growth simulations were performed on typical days of the year. The same approach as described in Pruvost et al. [42] for flat panel geometries (inclined plane, vertical or horizontal photobioreactors) was used. The irradiation conditions (direct light, diffuse light, incidence angle) obtained hour by hour for a summer day (July) and a winter day (January) for the Saint-Nazaire, France (47.25° N, 2.26°) region were thus used as a case study (Meteonorm software, Meteotest AG). Then, the current MCRT algorithm predicted the local rate of photon absorption $A(x,y)$ according to Eqs. (6) - (9). The temporal evolution of the biomass concentration was then deduced by assuming the volumetric growth rate $\langle r_X \rangle$ (11) to be constant over the time step Δt. The biomass concentration at time $t + \Delta t$ was calculated according to

$$C_X(t + \Delta t) = C_X(t) + \langle r_X \rangle \Delta t \tag{18}$$

PBR inclination angles β equal to 90° (vertical tube), 45° (inclined tube), and 0° (horizontal tube) with the tube centerline aligned with the North/South or East/West axis were simulated. Recall that only a single tube is considered, thus mutual shading between tubes is neglected. The PBR tube inner radius was set to r_i=0.03 m with a normalized tube thickness t/r_o=0.03 in the range of the optimal value as predicted previously (i.e. r_o=0.043 m). Initial biomass concentration was set to C_X =0.33 kg m^{-3} (i.e. corresponding to an optimal thickness C_X / a_{light} = 0.01 kg m^{-2}).

The temporal evolution of the biomass concentration and average growth rate is plotted in Figs. 14a, 14c and Figs. 14b, 14d for summer and winter days respectively. In all cases, a temporal evolution of biomass concentration typical of growth under solar conditions is

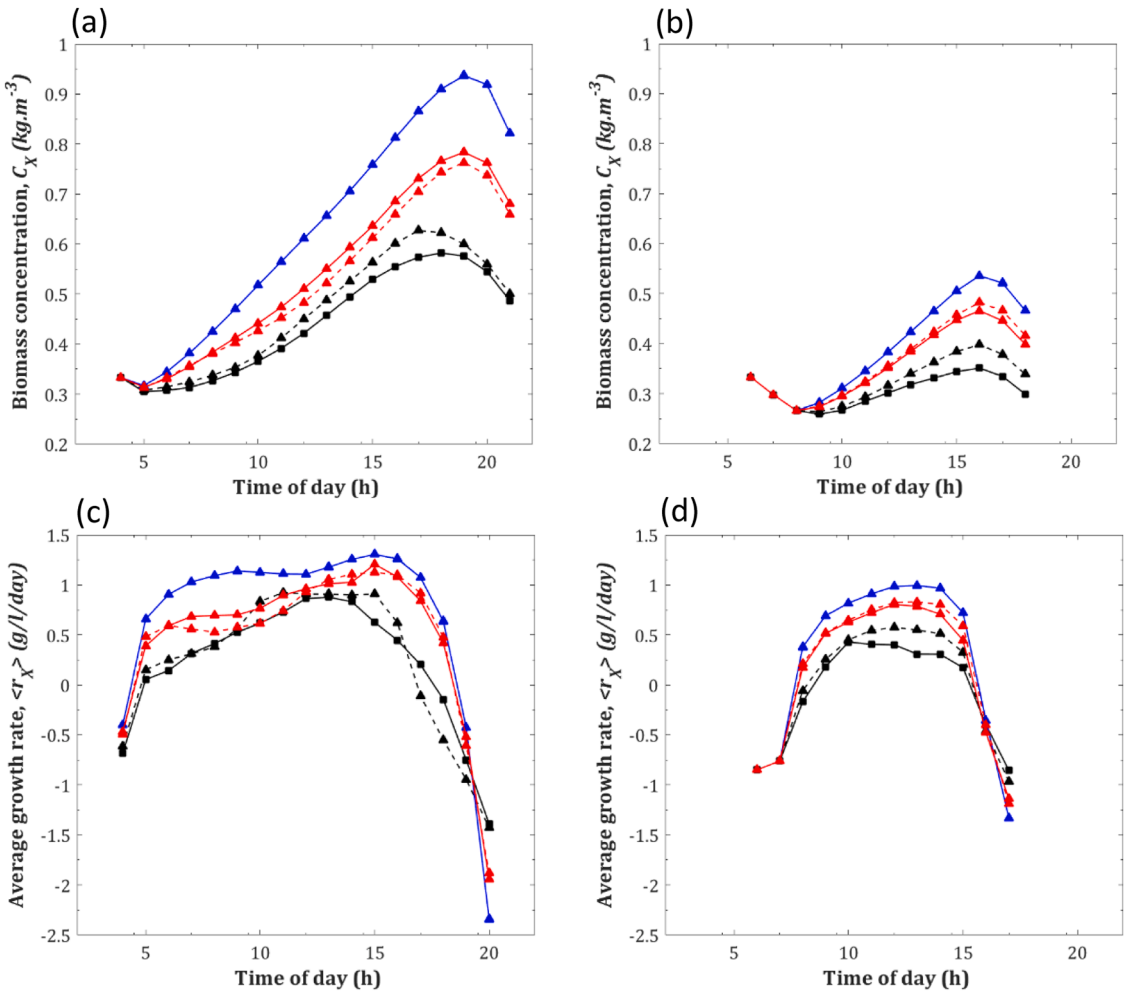

Fig. 14. Temporal evolutions of the biomass concentration C_X (a,b) and average volumetric growth rate $\langle r_X \rangle$ (c,d) for vertical (blue line), 45° (red lines) and horizontal (black lines) inclinations and for North/South (dashed lines) and East/West (solid lines) alignments. Results are given for solar conditions representative of a summer (a,b) and a winter day (c,d) respectively.

observed, with an increase in biomass concentration except during the first and last hours of the day where the low solar intensity leads to dark volumes (see also Figure 15a&b) resulting in a negative growth rate due to the contribution of respiratory activity over photosynthesis. A higher biomass concentration is obviously obtained for summer periods, as explained by longer days and a higher solar PFD in summer. This aspect has been described in detail in Pruvost et al. [46] and will not be discussed further.

More interestingly, vertical inclination leads to the best biomass growth rates and thus to the largest increase in biomass concentration. Compared to horizontal inclination, an increase of about 55 to 60 % in maximum biomass concentration is obtained with vertical inclination, with a 45° inclination leading to intermediate results between horizontal (+30 % approximately) and vertical inclination (-20 % approximately). Except for the last hours of the day (i.e. 20 h and 16 h for the summer and winter periods respectively), the average growth rate was always found to be higher for vertical PBR.

These results contrast with those of Pruvost et al [46]., who observed greater productivity for horizontal inclination with flat geometries during summer, due to a more favorable angle of incidence relative to the sun's path across the sky (i.e., a higher azimuth angle). For tubular PBRs, vertical inclination was consistently found to be better. This is explained by the effect of the tube curvature, which resulted in a more favorable evolution of the angle of incidence and the resulting light distribution in the tube compared to flat geometries. This is particularly demonstrated for the summer day, for which a more homogeneous temporal evolution of the growth rate is observed for most of the day for vertical inclination. After only a few hours after sunrise, the average growth rate is almost maximum and constant, which is less the case in all other cases. Unlike flat geometries, there is then no marked effect of the sun's low azimuth angle just after sunrise.

Another interesting result is that North/South and East/West alignments showed little influence on the growth rate obtained for a given inclination angle. For flat panel geometries, alignment is obviously crucial (the face not aligned with the sun's position will not receive direct radiation), with productivity being optimal when flat PBRs are oriented south. Due to the tube's curvature, PBR alignment modifies the light received and therefore productivity, but with a less pronounced effect. The main influence was observed for horizontal inclination, where East/West alignment proved more effective than North/South alignment.

To better illustrate the direct relationship with the light transfer conditions in the tubes, the temporal evolution of the illuminated light fraction (γ) and the mean photon absorption rate (MRPA) are shown in Figs. 15a, 15c and 15b, 15d for summer and winter days, respectively. Complex temporal evolutions of the illuminated light fraction and MRPA values were observed in all cases, because of both the interception of light with the tubes (i.e., intensity, angle of incidence) but also the variation of the biomass concentration during the day. The inclination of the tubes but also their alignment proved to be relevant here.

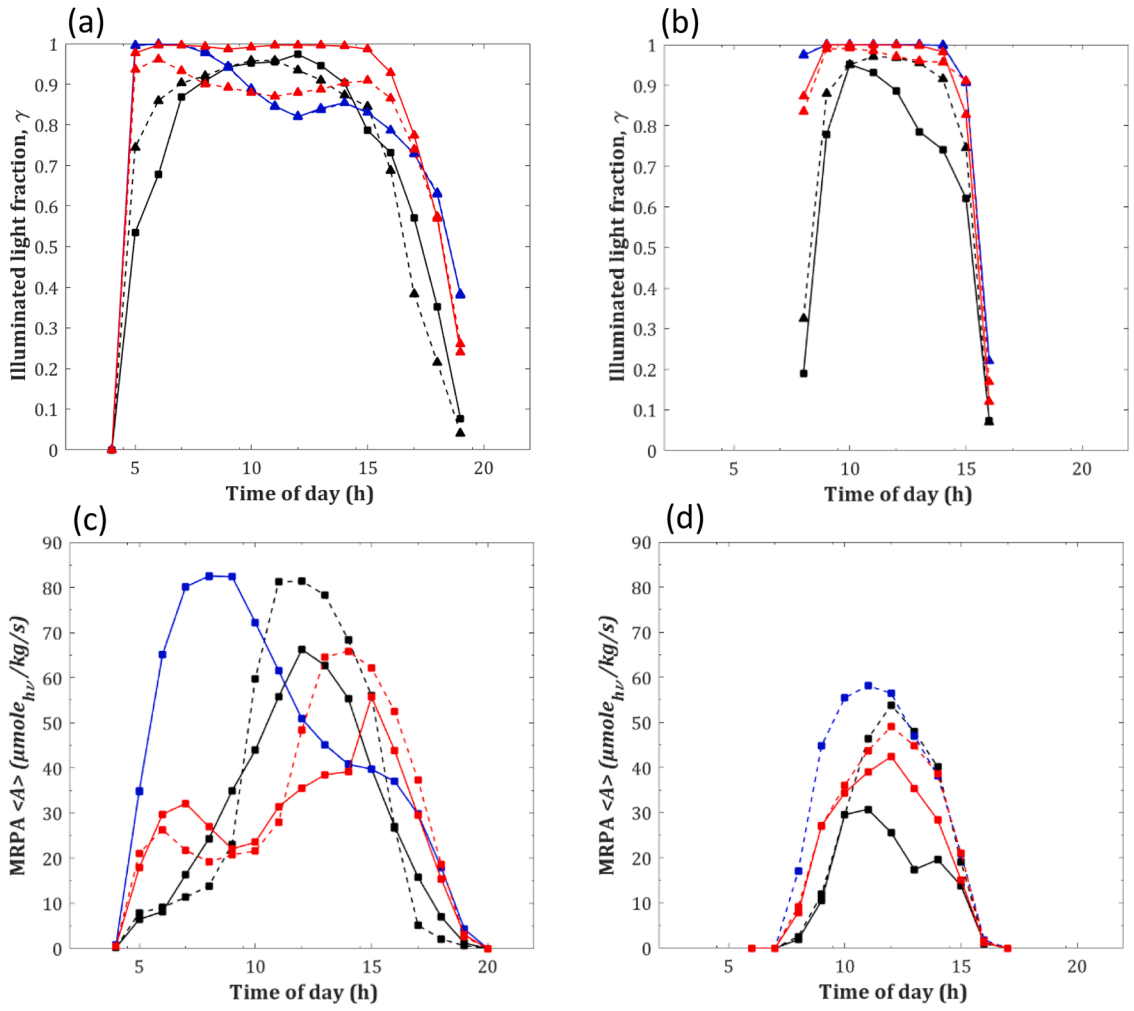

Fig. 15. Fig. 14: Temporal evolutions of the illuminated light fraction γ (a,b) and mean rate of photons absorption MRPA (c,d) for vertical (blue line), 45° (red lines) and horizontal (black lines) inclinations and for North/South (dashed lines) and East/West (solid lines) alignments. Results are given for solar conditions representative of a summer (a,b) and a winter day (c,d) respectively.

For example, the entire culture volume was found illuminated at sunrise for both vertical and 45° inclinations (γ close to 1), although the horizontal inclination presented dark volumes ($\gamma < 1$), with an illuminated light fraction already below 1 at sunrise (i.e., in the range 0.5–0.7 and 0.2–0.3 for summer and winter days respectively). This is in direct relation to the growth rate and the evolution of the biomass concentration. For example, a clear decrease in the illuminated fraction γ of the vertical PBR (Fig. 15-a) was observed at midday for the summer day, which led to a notable decrease in the biomass growth rate (Fig. 14-b). As another example, the previous comparison between the North/South and East/West alignments for the horizontal inclination reveals that the North/South alignment is less efficient. This was due to the large incidence angles in the morning for the North/South alignment that decreased the illuminated fraction γ (Fig. 15-a) and so the growth rate (Fig. 14-b).

Several studies have demonstrated the direct link between MRPA and photosynthetic response. Thus, excessively high MRPA values lead to oversaturation of the photosynthetic apparatus, which can lead to growth rate reduction (also called photoinhibition, not considered in our growth model). For example Bonnanfant et al. [47] demonstrated the direct relationship between photosynthetic activity, light sensitivity, and pigment acclimation of microalgae with MRPA values. MRPA values above 60 $\mu mole_{h\nu}.kg_x^{-1}.\ s^{-1}$ were found to lead to a significant decrease in photosynthetic activity in *Chlorella vulgaris* culture. Figs. 15c and 15d highlight the rapid evolution of MRPA values during a day. Depending on the tube inclination, the peak MRPA value occurred at different times of the day (from morning to late afternoon in summer). High values were obtained in summer ($> 80 \mu mole_{h\nu}.kg_x^{-1}.\ s^{-1}$ for vertical and horizontal PBRs) but also in winter due to lower biomass concentration (up to about 60 $\mu mole_{h\nu}.kg_x^{-1}.\ s^{-1}$ for vertical inclination). Tube alignment was found to be more sensitive to horizontal inclination. North/south alignment led to higher and then lower dark volumes than east/west alignment in the first and last hours of the day, respectively. But the illuminated light fraction was rather similar for most of the day in summer, but with a very different profile in winter, especially for the north/south alignment with the largest values of dark volume during the day. However, this also produces the lowest MRPA values (below 30 $\mu mole_{h\nu}.kg_x^{-1}.\ s^{-1}$), with the lowest light stress conditions among the different cases simulated here. For the vertical inclination case, although it corresponds to the maximum growth rate, it also resulted in the highest MRPA value reached here, with then potential light stress. As shown in Fig. 15c, the few hours after sunrise were already subjected to the greatest light stress here, with then very high MRPA values maintained for several hours. Such conditions could lead to growth problems when cultivating photosensitive strains.

5. Conclusion

A Monte Carlo Ray Tracing (MCRT) method was developed to simulate light transfer in tubular PBRs taking into account diffuse and

collimated incident solar radiation, multiple reflection and refraction at all optical interfaces, as well as anisotropic scattering and absorption by the microalgae cells in suspension. The MCRT algorithm was used to conduct a detailed numerical analysis of light transfer in tubular PBRs and to assess the impact of various parameters. First, the study establishes that scattering by the microalgae in tubular PBRs must be accounted for, unlike in flat panel PBRs when it could be neglected. Our analysis also confirmed that the volume fraction γ of the tubular PBR sufficiently illuminated to support microalgae growth was an essential parameter to assess PBR performance. The study established that γ scaled with the tube wall thickness t normalized by the tube outer radius r_0 and with the optical thickness $C_X r_i$ of the microalgae suspension for a given incident photon flux density. These scaling relationships enabled us to connect the areal growth rate and the volume fraction γ to essential design and operating parameters $t/r_0$and $C_X r_i$ for scaling and optimizing solar tubular PBRs.

Furthermore, γ was found to increase with increasing t/r_o due to refraction by the tube walls resulting in light concentration which increased the photon flux density entering the culture. This concentration effect was more pronounced at larger incidence angles θ_{in} when the sun was high in the sky for a solar PBR using vertical tubes, or when the sun was low on the horizon for horizontal tubes with tube centerline aligned with East/West axis, for example.

The concave PBR wall resulted in less efficient light to biomass conversion in tubular PBRs than in flat panel PBRs under similar illumination conditions, resulting in a difference in areal growth rate of around 20–30 % for collimated light and similar incident angle. The different was less significant under diffuse incident radiation. It was also interesting to note that, unlike in flat PBRs, the optimal light conditions of $\gamma = 1$ – corresponding to optimal kinetic performance with full light absorption and no dark volume – did not coincide with maximal growth rate in tubular PBRs, because of the complex light attenuation field induced by tube wall curvatures. The latter resulted in larger dark volume or excessive local rate of photon absorption near the wall, both leading to lower photosynthetic conversion.

The biomass growth rate for several tubular PBR inclinations and orientations was predicted for realistic solar conditions during Winter and Summer in Saint-Nazaire, France. Unlike flat panel PBRs, for which higher productivity was observed for horizontal inclination in the summer, vertical tubular PBRs achieved a maximum biomass concentration 55–60 % larger than in horizontal inclination. After only a few hours after sunrise, the average growth rate had reach its maximum and was constant. An analysis of the rate of photons absorption by the culture showed that, regardless of conditions (inclination, orientation, period of the year), tubular PBRs could exhibit significant variations in mean rate of photon absorption (MRPA), larger than those observed in flat panel PBRs for similar conditions. This was particularly true for vertical inclination, which creates the most stressful lighting conditions, with MRPA above 80 $\mu mole_{h\nu}.kg_x^{-1}$.

Finally, the open-source MCRT code can be modified to incorporate aspects not considered in the present study such as: (i) fouling or biofilm formation on the tube walls, (ii) multi-tubes configurations, or (iii) the presence of bubbles (e.g., in a vertical airlift PBR) or of air-liquid interface in wavy flows (e.g., PBR Lgem). Note that some of these aspects have already been considered in literature [39,40]. To decrease the computational time, the open source MCRT code could also be optimized by integrating the latest advances in high performance computing for radiative transfer Monte Carlo with efficient algorithms designed based on integral formulation. It can also use scientific computation libraries developed by computer graphics research for accelerating ray tracing in complex systems at the industrial scale [27, 48–50].

Supplementary material

The MCRT source code is available as supplementary material (Matlab file). The last version is also available via a public share on GitHUB:

https://github.com/JeremyPruvost/MCRT-for-tubular-photobioreactor

Funding information

This research was supported by the DISCUS project of the NExT Initiative (Nantes Excellence Trajectory) International Research Partnership.

CRediT authorship contribution statement

J. Hoeniges: Writing – original draft, Software, Investigation, Formal analysis. **L. Pilon:** Writing – review & editing, Supervision, Conceptualization. **J. Dauchet:** Writing – review & editing, Validation, Methodology. **J. Pruvost:** Writing – review & editing, Validation, Supervision, Software, Methodology, Investigation, Conceptualization.

Declaration of competing interest

Authors declare there are no potential financial or other interests that could be perceived to influence the outcomes of the research.

Acknowledgments

Funding: this research was supported by the DISCUS project of the NExT Initiative (Nantes Excellence Trajectory) International Research Partnership.

Supplementary materials

Supplementary material associated with this article can be found, in the online version, at doi:10.1016/j.ceja.2026.101081.

Appendix

Calculation of the photons flux density $\boldsymbol{q''_{in}}$ averaged on the tubular PBR surface facing the sun

Following Fig. 1, the local PFD received at a given position on the tube outer surface for a collimated light is:

$$q''_{col} = I_{col}\cos\theta \tag{A1}$$

where θ is the angle between the unit vectors defining the incoming collimated radiation $\vec{e}_{in} = \langle \cos\theta_{in},\ 0, -\sin\theta_{in} \rangle_{(x,y,z)}$ and the normal of the tube surface $\vec{n}(\vec{y}) = \langle -\cos\alpha, -\sin\alpha,\ 0 \rangle_{(x,y,z)}$ given by:

$$\cos\theta = \vec{e}_{in} \cdot \vec{n}(\vec{y}) = -\cos\theta_{in}\cos\alpha \tag{A2}$$

With then:

$$q''_{col}(\vec{y}) = \mathrm{I}_{col}\, \vec{e}_{in} . \vec{n}(\vec{y}) \tag{A3}$$

The average collimated flux onto the tube outer surface S_{light} receiving sunlight (half the tube) can then be given by:

$$\overline{q}''_{col} = \frac{1}{S_{light}} \int_{S_{light}} q''_{col}(\vec{y})\mathrm{dS}(\vec{y}) = \frac{1}{\pi r H} \int_0^H dz \int_{\pi/2}^{3\pi/2} q''_{col}(\vec{y}) r d\alpha$$

$$= \frac{1}{\pi} \int_{\pi/2}^{3\pi/2} \mathrm{I}_{col}\left(\vec{e}_{in} . \vec{n}(\vec{y})\right) d\alpha = -\frac{1}{\pi} \int_{\pi/2}^{3\pi/2} \mathrm{I}_{col}\cos\theta_{in}\cos\alpha d\alpha$$

$$= \frac{-\mathrm{I}_{col}}{\pi}\cos\theta_{in} \int_{\pi/2}^{3\pi/2} \cos\alpha d\alpha = \frac{-\mathrm{I}_{col}}{\pi}\cos\theta_{in}[\sin\alpha]_{\pi/2}^{3\pi/2}$$

$$= \frac{2}{\pi}\mathrm{I}_{col}\cos\theta_{in} \tag{A4}$$

The average diffuse flux onto the tube outer surface can be given by:

$$\overline{q}''_{dif} = \int_0^{2\pi}\int_0^{\pi/2} \mathrm{I}_{dif}(\theta,\varphi)\cos\theta\sin\theta d\theta d\varphi$$

$$= \mathrm{I}_{dif} \int_0^{2\pi}\int_0^{\pi/2} \cos\theta\sin\theta d\theta d\varphi$$

$$= \mathrm{I}_{dif} \int_0^{2\pi} d\varphi \int_0^{\pi/2} \cos\theta\sin\theta d\theta$$

$$= 2\pi\mathrm{I}_{dif} \int_0^{\pi/2} \cos\theta\sin\theta d\theta$$

$$= 2\pi\left(\frac{1}{2}\right)\mathrm{I}_{dif}$$

$$= \pi\mathrm{I}_{dif} \tag{A5}$$

Data availability

The model will be made available to the community as an open source code via a public share on GitHUB (https://github.com/JeremyPruvost/MCRT-for-tubular-photobioreactor.git)

References

[1] Intergovernmental Panel on Climate Change, Climate Change 2022: Impacts, Adaptation and Vulnerability., Cambridge University Press, Cambridge University Press, Cambridge, UK and New York, NY, USA, 2023.

[2] J. Matos, C. Cardoso, N.M. Bandarra, C. Afonso, Microalgae as healthy ingredients for functional food: a review, Food Funct. 8 (2017) 2672–2685.

[3] Y. Chisti, Biodiesel from microalgae, Biotechnol. Adv. 25 (2007) 294–306.

[4] D. Jha, V. Jain, B. Sharma, A. Kant, V.K. Garlapati, Microalgae-based pharmaceuticals and nutraceuticals: an emerging field with immense market potential, ChemBioEng Rev. 4 (2017) 257–272.

[5] M. Tredici, Mass production of photobioreactors, in: A. Richmond (Ed.), Handbook of Microbial Culture, Biotechnology and Applied Phycology, Blackwell science, 2004, pp. 178–214.

[6] J. Pruvost, J.F. Cornet, L. Pilon, Large scale production of algal biomass: photobioreactors, in: U. Springer (Ed.), Algae Biotechnology: Products and Processes, 2016, pp. 41–66.

[7] L. Pilon, H. Berberoglu, R. Kandilian, Radiation transfer in photobiological carbon dioxide fixation and fuel production by microalgae, J. Quant. Spectrosc. Radiat. Transf. 112 (2011) 2639–2660.

[8] R. Kandilian, A. Taleb, V. Heredia, G. Cogne, J. Pruvost, Effect of light absorption rate and nitrate concentration on TAG accumulation and productivity of Parachlorella kessleri cultures grown in chemostat mode, Algal Res. 39 (2019) 101442.

[9] P. Santos Corrêa, W. Galvão de Morais Júnior, N. de Sá Caetano, tubular photobioreactors applied to algal production. Elsevier (Ed.) Algal Bioreactors: Science, Engineering and Technology of Upstream Processes, Woodhead Publishing, 2024, pp. 407–421.

[10] J. Pruvost, F. Le Borgne, A. Artu, J.-F. Cornet, J. Legrand, Industrial photobioreactors and scale-up concepts. Advances in Chemical Engineering - Photobioreaction Engineering, Elsevier, 2016, pp. 257–310.

[11] A. Soulies, C. Castelain, T.I. Burghelea, J. Legrand, H. Marec, J. Pruvost, Investigation and modeling of the effects of light spectrum and incident angle on the growth of *chlorella vulgaris* in photobioreactors, Biotechnol. Prog. 32 (2016) 247–261.

[12] L. Li, Z.M.H. Mohd Shafie, T. Huang, R. Lau, C.-H. Wang, Multiphysics simulations of concentric-tube internal loop airlift photobioreactors for microalgae cultivation, Chem. Eng. J. 457 (2023) 141342.

[13] J. Pruvost, F. Le Borgne, A. Artu, J. Legrand, Development and characterization of a thin-film solar photobioreactor (AlgoFilm©) based on process intensification principles, Algal Res. (2017) 120–137.

[14] L. Pottier, J. Pruvost, J. Deremetz, J.F. Cornet, J. Legrand, C.G. Dussap, A fully predictive model for one-dimensional light attenuation by Chlamydomonas reinhardtii in a torus photobioreactor, Biotechnol. Bioeng. 91 (2005) 569–582.

[15] E. Lee, J. Pruvost, X. He, R. Munipalli, L. Pilon, Design tool and guidelines for outdoor photobioreactors, Chem. Eng. Sci. 106 (2014) 18–29.
[16] J.F. Cornet, C.G. Dussap, P. Cluzel, G. Dubertret, A structured model for simulation of cultures of the cyanobacterium Spirulina platensis in photobioreactors. 1. Coupling between light transfer and growth kinetics, Biotechnol. Bioeng. 40 (1992) 817–825.
[17] J. Pruvost, J.F. Cornet, Knowledge models for engineering and optimization of photobioreactors, in: C.P.a. C.Walter (Ed.), Microalgal Biotechnology, De Gruyter GmbH & Co. KG, 2012, pp. 181–224.
[18] J.F. Cornet, C.G. Dussap, J.B. Gros, A simplified monodimensional approach for modeling coupling between radiant light transfer and growth kinetics in photobioreactors, Chem. Eng. Sci. 50 (1995) 1489–1500.
[19] H. Takache, G. Christophe, J.F. Cornet, J. Pruvost, Experimental and theoretical assessment of maximum productivities for the microalgae Chlamydomonas reinhardtii in two different geometries of photobioreactors, Biotechnol. Prog. 26 (2010) 431–440.
[20] P.M. Slegers, P.J.M. van Beveren, R.H. Wijffels, G. van Straten, A.J.B. van Boxtel, Scenario analysis of large scale algae production in tubular photobioreactors, Appl. Energy 105 (2013) 395–406.
[21] X. He, L. Lee, L. Wilcox, R. Munipalli, L. Pilon, A high-order-accurate gpubased radiative transfer equation solver for combustion and propulsion applications, Numer. Heat Transf. B: Fundam. 63 (2013) 457–484.
[22] J. Hoeniges, W. Welch, J. Pruvost, L. Pilon, A novel external reflecting raceway pond design for improved biomass productivity, Algal Res. 65 (2022) 102742.
[23] G. Marotta, J. Pruvost, F. Scargiali, G. Caputo, A. Brucato, Reflection-refraction effects on light distribution inside tubular photobioreactors, Can. J. Chem. Eng. (2017).
[24] R. Laifa, J. Morchain, L. Barna, P. Guiraud, A numerical framework to predict the performances of a tubular photobioreactor from operating and sunlight conditions, Algal Res. 60 (2021) 102550.
[25] J. Pruvost, MCRT-for-tubular-photobioreactor, GitHub, 2025. https://github.com/JeremyPruvost/MCRT-for-tubular-photobioreactor.
[26] R. Kandilian, J. Pruvost, A. Artu, C. Lemasson, J. Legrand, L. Pilon, Comparison of experimentally and theoretically determined radiation characteristics of photosynthetic microorganisms, J. Quant. Spectrosc. Radiat. Transf. 175 (2016) 30–45.
[27] J. Dauchet, S. Blanco, J.F. Cornet, M. El Hafi, V. Eymet, R. Fournier, The practice of recent radiative transfer Monte Carlo advances and its contribution to the field of microorganisms cultivation in photobioreactors, J. Quant. Spectrosc. Radiat. Transf. 128 (2013) 52–59.
[28] J. Hoeniges, K. Zhu, J. Pruvost, J. Legrand, E.-k. Si-Ahmed, L. Pilon, Impact of dropwise condensation on the biomass production rate in covered raceway ponds, Energies 14 (2021) 268.
[29] Y. Huang, C. Feng, J. Hoeniges, K. Zhu, L. Pilon, Bidirectional transmittance of transparent windows with external or backside condensation of nonabsorbing cap-shaped droplets, J. Quant. Spectrosc. Radiat. Transf. 251 (2020) 107039.
[30] K. Zhu, L. Pilon, Transmittance of semitransparent windows with non-absorbing cap-shaped droplets condensed on their backside, J. Quant. Spectrosc. Radiat. Transf. 194 (2017).
[31] K. Zhu, S. Li, L. Pilon, Light transfer through windows with external condensation, J. Quant. Spectrosc. Radiat. Transf. 208 (2018) 164–171.
[32] R.A. Yalcln, E. Blandre, K. Joulain, J. Dévrillon, Colored radiative cooling coatings with nanoparticles, ACS Photonics 7 (2020) 1312–1322.
[33] Y. Soriano-Jerez, J.J. Gallardo-Rodriguez, L. Lopez-Rosales, F. Garcia-Camacho, C. Bressy, E. Molina-Grima, M.C. Ceron-Garcia, Preventing biofouling in microalgal photobioreactors, Bioresour. Technol 407 (2024) 131125.
[34] R. Descartes, La Dioptrique, in: C.J.-. Philosophies (Ed.), Oeuvres Philosophiques, Tome I -, pp. 1618...1637.
[35] A.J. Fresnel, Mémoire sur la loi des modifications que la réflexion imprime à la lumière polarisée - reflection impresses on polarized light, in: A.d. Sciences (Ed.) 1823.
[36] J. Pruvost, J.F. Cornet, V. Goetz, J. Legrand, Theoretical investigation of biomass productivities achievable in solar rectangular photobioreactors for the cyanobacterium *Arthrospira platensis*, Biotechnol. Prog. 28 (2012) 699–714.
[37] J. Hoeniges, R. Kandilian, C. Zhang, J. Pruvost, J. Legrand, D. Grizeau, L. Pilon, Effect of colony formation on light absorption by botryococcus braunii, Algal Res. 50 (2020) 101985.
[38] J.F. Cornet, C.G. Dussap, J.B. Gros, Conversion of radiant light energy in photobioreactors, AIChE J. 40 (1994) 1055–1066.
[39] Y. Zheng, L. Li, S. Dai, D. Liu, H. Zheng, S. Yang, Y. Guo, M. Rafique, B. Wang, C. H. Wang, Y. Shuai, Monte-Carlo ray tracing simulation of view factors for diffuse solar radiation determination in cylindrical photobioreactor arrays for microalgae cultivation, Bioresour. Technol. 436 (2025) 132813.
[40] V. Pozzobon, Impact of bubbles on the light field within a photobioreactor: A practical design tool, Algal Res. 91 (2025) 104331.
[41] J.F. Cornet, C.G. Dussap, A simple and reliable formula for assessment of maximum volumetric productivities in photobioreactors, Biotechnol. Prog. 25 (2009) 424–435.
[42] J. Pruvost, J.F. Cornet, F. Le Borgne, V. Goetz, J. Legrand, Theoretical investigation of microalgae culture in the light changing conditions of solar photobioreactor production and comparison with cyanobacteria, Algal Res. 10 (2015) 87–99.
[43] R. Kandilian, A. Soulies, J. Pruvost, B. Rousseau, J. Legrand, L. Pilon, Simple method for measuring the spectral absorption cross-section of microalgae, Chem. Eng. Sci. 146 (2016) 357–368.
[44] J. Pruvost, R. Rasheed, K. Samhat, A. Kazbar, H. Al Jabri, J. Dauchet, J.F. Cornet, A simple new approach predicting how microalgae culture systems will perform under sunlight and artificial light conditions, Algal Res. 80 (2024) 103517.
[45] H. Takache, J. Pruvost, J.F. Cornet, Kinetic modeling of the photosynthetic growth of chlamydomonas reinhardtii in a photobioreactor, Biotechnol. Prog. 28 (2012) 681–692.
[46] J. Pruvost, J.F. Cornet, V. Goetz, J. Legrand, Modeling dynamic functioning of rectangular photobioreactors in solar conditions, AIChE J. 57 (2011) 1947–1960.
[47] M. Bonnanfant, H. Marec, B. Jesus, J.-L. Mouget, J. Pruvost, Investigation of the photosynthetic response of Chlorella vulgaris to light changes in a torus-shape photobioreactor, Appl. Microbiol. Biotechnol. 105 (2021) 8689–8701.
[48] J. Delatorre, G. Baud, J.J. Bézian, S. Blanco, C. Caliot, J.F. Cornet, C. Coustet, J. Dauchet, M. El Hafi, V. Eymet, R. Fournier, J. Gautrais, O. Gourmel, D. Joseph, N. Meilhac, A. Pajot, M. Paulin, P. Perez, B. Piaud, M. Roger, J. Rolland, F. Veynandt, S. Weitz, Monte Carlo advances and concentrated solar applications, Sol. Energy 103 (2014) 653–681.
[49] N. Villefranque, R. Fournier, F. Couvreux, S. Blanco, C. Cornet, V. Eymet, V. Forest, J.M. Tregan, A path-tracing Monte Carlo library for 3-D radiative transfer in highly resolved cloudy atmospheres, J. Adv. Model. Earth Syst. 11 (2019) 2449–2473.
[50] I. Wald, S. Woop, C. Benthin, G.S. Johnson, M. Ernst, Embree, ACM Trans. Graph. 33 (2014) 1–8.